Volume 16
Number 5
May 2025
Pages 1845–2298

RSC Medicinal Chemistry

rsc.li/medchem

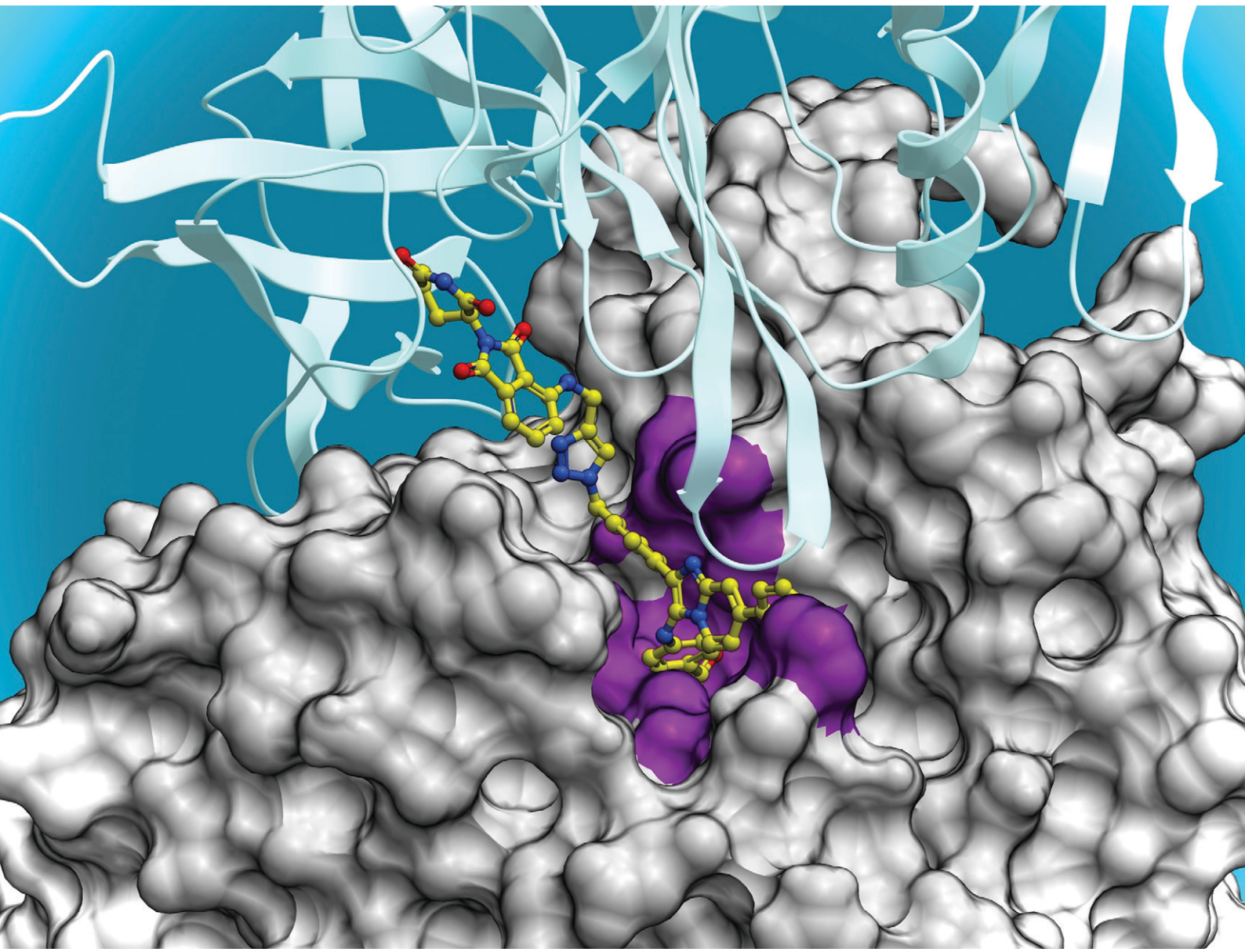

ISSN 2632-8682

ROYAL SOCIETY OF CHEMISTRY

RESEARCH ARTICLE
Xue Zhi Zhao *et al.*
Application of a bivalent "click" approach to target tyrosyl-DNA phosphodiesterase 1 (TDP1)

RSC Medicinal Chemistry

ROYAL SOCIETY OF CHEMISTRY

RESEARCH ARTICLE

View Article Online
View Journal | View Issue

Cite this: *RSC Med. Chem.*, 2025, **16**, 1969

Application of a bivalent "click" approach to target tyrosyl-DNA phosphodiesterase 1 (TDP1)†

Xue Zhi Zhao, *[a] Wenjie Wang, [b] Md Rasel Al Mahmud, [b] Keli Agama, [b] Yves Pommier[b] and Terrence R. Burke Jr. [a]

Received 22nd October 2024,
Accepted 26th January 2025

DOI: 10.1039/d4md00824c

rsc.li/medchem

Although inhibiting the DNA repair enzyme tyrosyl-DNA phosphodiesterase 1 (TDP1) synergizes with topoisomerase type I (TOP1) inhibitors in anticancer therapy, development of TDP1 inhibitors has been highly challenging. This may be due to the open and shallow nature of the TDP1 catalytic site and the necessity of competing with a large and highly extended substrate. The toolbox available to chemical biologists for studying TDP1 could be significantly enhanced by introducing the ability to selectively eliminate TDP1 using protein degraders. Our current work starts from phenyl imidazopyridine-based TDP1 inhibitors previously developed from small molecule microarrays (SMMs). Using crystal structures of lead inhibitors bound to TDP1, we designed and synthesized a series of bivalent proteolysis-targeting chimeras (PROTACs). The focus of our current work is to explore synthetic approaches that permit installation of E3 ligase-targeting functionality, while retaining the TDP1 binding. We employed copper-catalyzed azide–alkyne cycloaddition (CuAAC) "click" reactions to assemble PROTAC constituents with 1,2,3-triazole-containing linkers. With the addition of the relatively large parts of the linkers and E3-targeting moieties, we retained the ability to inhibit TDP1. The successful development of TDP1-directed PROTACS would yield a new therapeutic class that could potentially enhance the efficacy and selectivity of TOP1 inhibitors including those used as payloads in antibody drug conjugates (ADCs).

Introduction

DNA repair enzymes are targets for anticancer therapy. DNA supercoiling can occur during replication and transcription and numerous other important cellular processes.[1] Enzymes, such as topoisomerases, regulate the degree of DNA supercoiling. The human topoisomerase type I (TOP1) supresses supercoiling by relaxing the DNA helix.[2] TOP1 removes supercoils by forming single-strand DNA breaks in a reversible process, which involves the nucleophilic attack of the TOP1 catalytic tyrosyl Y723 hydroxyl onto the phospho-backbone of a target DNA chain to form a 3′-phosphodiester bond with release of the 5′-terminal chain. The resulting covalent TOP1–DNA cleavage complex (TOP1cc) permits the freed 5′-DNA end to undergo rotation and relax supercoils. Once supercoiling has been removed, the cut DNA 5′-strand can attack the 3′-end phosphotyrosyl bond to regenerate the DNA backbone and release TOP1.[3] This process is the target of anticancer drugs, such as the TOP1 inhibitors irinotecan and topotecan, and their derivative exatecan used in antibody drug conjugates (ADCs), as they trap TOP1cc intermediates. Subsequent double-strand breaks kill cancer cells.[4] The DNA repair enzyme tyrosyl-DNA phosphodiesterase 1 (TDP1) hydrolyzes phosphodiester bonds between 3′-terminal DNA-phosphates.[5,6] Human TDP1 is a 608 residues 68 kDa enzyme that serves important roles in repairing DNA lesions by hydrolyzing phosphodiester bonds between DNA 3′-phosphates and a diversity of adducts.[4,7] In cells, TDP1 hydrolyzes phosphodiester bonds of nicked double-stranded DNA (dsDNA) linked to polypeptides that result from proteolytic digestion of TOP1cc complexes.[8–10] Cleavage of the phosphodiester bond between the TOP1 Y723 residue and the DNA 3′-phosphate group takes place after proteolytic degradation of the TOP1ccs. By cleaving these phosphodiester bonds and enabling DNA repair, TDP1 limits the effectiveness of TOP1 inhibitors.[5,11–13] Genetic inactivation of TDP1 blocks the degradation of therapeutically critical TOP1–DNA adducts and synergizes with TOP1-targeted drugs.[14,15] Importantly, loss of TDP1 function is well tolerated in preclinical models.[16] Thus, chemical inhibition of TDP1 could potentially retard the degradation of

[a] *Chemical Biology Laboratory, Center for Cancer Research, National Cancer Institute, Frederick, MD, USA. E-mail: xuezhi.zhao@nih.gov*
[b] *Developmental Therapeutics Branch & Laboratory of Molecular Pharmacology, Center for Cancer Research, National Cancer Institute, Bethesda, MD, USA*
† Electronic supplementary information (ESI) available. See DOI: https://doi.org/10.1039/d4md00824c

therapeutically critical TOP1ccs induced by TOP1 inhibitors and increase their anticancer activity.[7,15,17,18] This has made development of TDP1 inhibitors a compelling line of research. Development of TDP1 inhibitors is made highly challenging by the open and shallow nature of the TDP1 catalytic site.

Although TDP1 inhibitors are recognized as valid therapeutic targets for use with TOP1 inhibitors,[6] there are no TDP1 inhibitors currently in clinical trials. This may be due to the challenges posed by the open and shallow nature of the TDP1 catalytic site.[12,19–24] As a member of the phospholipase D (PLD) superfamily, the TDP1 catalytic apparatus contains conserved groups of histidine, lysine, and asparagine residues in close proximity (HKN motifs, H263/K265/N283 and H493/K495/N516) (Fig. 1C). These form a conserved catalytic pocket, in which a nucleophilic attack is mediated on the substrate 3′-DNA phosphodiester bond.[12,25] The nature of the catalytic machinery was revealed by crystal structures of the TDP1 (Δ1–148) C-terminal domain bound to a complex of TOP1-derived peptide, DNA substrate and a vanadate transition state mimetic (PDB code: 1NOP) (Fig. 1B).[12,19,25,26] These structures highlight a three-component architecture consisting of a substrate DNA strand (green sticks in Fig. 1B), a tyrosyl-containing peptide

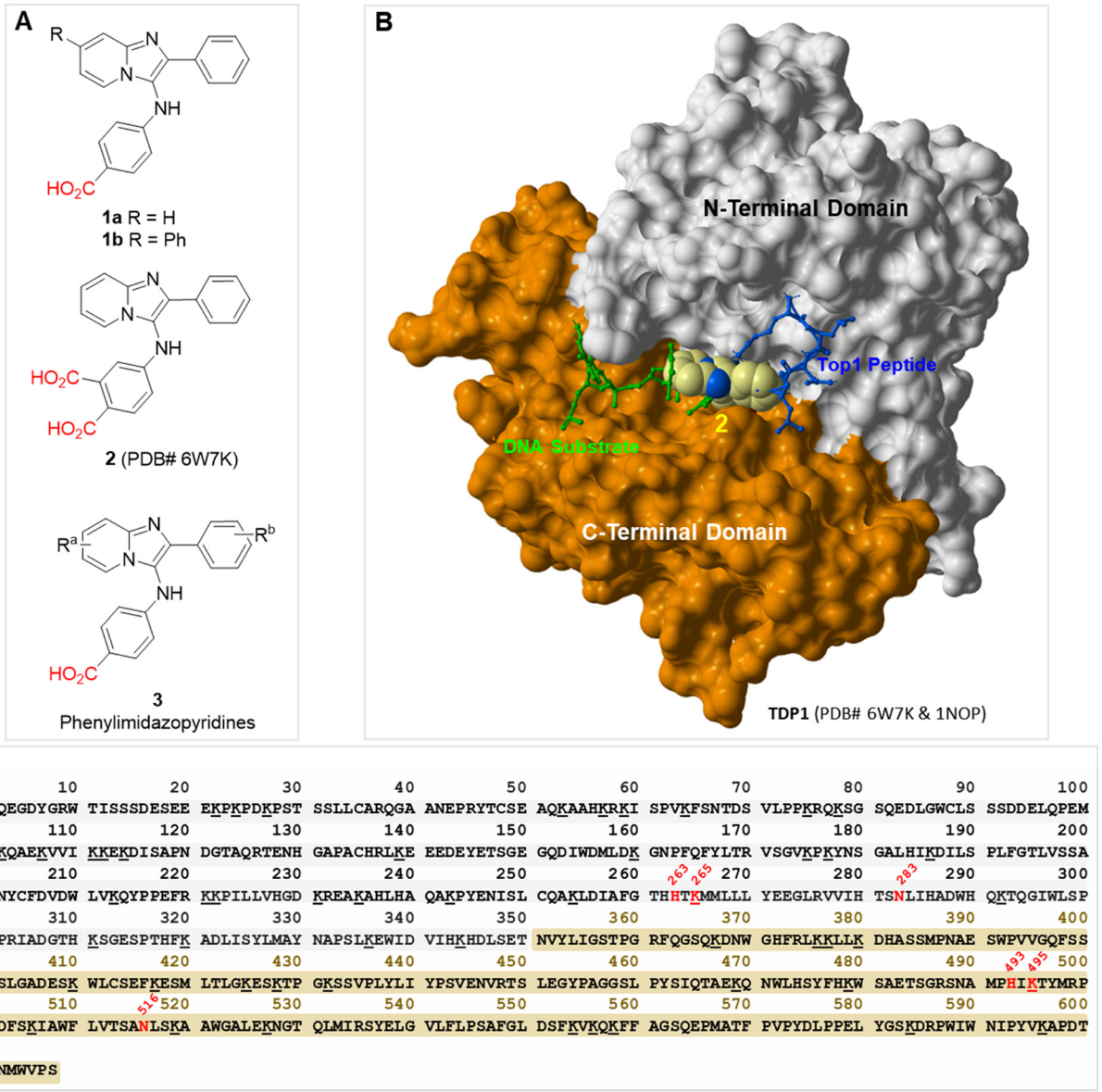

Fig. 1 Structures of imidazopyridine TDP1 inhibitors and the TDP1 enzyme. (A) Structures of lead imidazopyridine TDP1 inhibitors (**1**–**3**). (B) Crystal structure surface rendering of TDP1(Δ1–148) with compound **2** bound in the catalytic pocket (PDB code: 6W7K). A vanadate complex of a TOP1-derived peptide (blue sticks) and DNA substrate (green sticks) (PDB code: 1NOP) are superimposed as mimics of phospho-substrate. The surfaces of N-terminal domain residues (149–350) and C-terminal domain residues (351–608) are shown in grey and brown, respectively. (C) The amino acid sequence of human TDP1 with the N-terminal and C-terminal domain residues 1–350 and 351–608 highlighted in black and tan, respectively. Positions of the catalytic 'HKN' motifs are highlighted in red and lysine residues (52 in total) are underlined.

(blue sticks in Fig. 1B) and a vanadate moiety in middle that serves to mimic the geometry of the TDP1-bound phosphate transition state complex. The three major binding components of the substrate are defined by (1) the bottom of catalytic cleft formed by the two HKN motifs; (2) an extended positively charged cleft extending from one side of the active site along which lays a single-stranded DNA (green sticks in Fig. 1B) bearing the 3′-phospho adduct and (3) a more open region that accommodates the TOP1-derived peptide (blue sticks in Fig. 1B) that projects from the catalytic pocket in a direction opposite to the DNA-binding channel. Although the phospho-binding pocket is well defined, it is relatively shallow as are the open, extended topologies of the DNA and peptide-binding regions. The large macromolecular nature of the substrate and the shallow catalytic pocket pose challenges to developing potent TDP1 inhibitors.[27,28] After significant effort, several groups have reported a spectrum of structurally diverse TDP1 inhibitors. These include natural product-derived inhibitors,[29–39] noncompetitive inhibitors,[38,40,41] potential allosteric peptide inhibitors,[42] and irreversible inhibitors.[40,43] The structural bases for how these inhibitors interact with TDP1 are generally unknown and many reported TDP1 inhibitors exhibit physiochemical properties that could potentially endow them with promiscuous mechanisms of inhibition, which would make them of questionable value for further development.[44]

In a qualitative departure from previous efforts, we interrogated the ability of ligands to bind to TDP1 using a small molecule microarray (SMM) of more than 20 000 ligands. This led to the identification of 2-phenylimidazo[1,2-*a*]pyridines as TDP1-binding motifs (**1a**, **1b** and **2**, Fig. 1A).[22] More recently, we applied oxime diversification strategies to a subset of these SMM-derived platforms to develop trivalent ligands (**3**) intended to engage residues within TDP1's catalytic pocket, while extending into the DNA and peptide-binding channels.[24] X-ray crystal structure of inhibitor **2** bound within the TDP1 catalytic pocket shows that key inhibitor carboxylic acid groups form hydrogen bonds with residues of the catalytic HKN motif (Fig. 1B and 2B). The pyridine rings of the imidazopyridine unit point toward the relatively narrow and positively charged DNA–substrate-binding pocket, while the phenyl rings are directed toward the TOP1-peptide binding pocket (Fig. 1B).

Bivalent constructs have been designed to simultaneously bind distinct domains on two different targets

Proteolysis-targeting chimeras (PROTACs) employ bivalent constructs that bring into proximity a target protein and a degradation component. This can lead to the targeted degradation of the protein (Fig. 2A).[45] One element of the PROTAC binds specifically to a protein that is the target of degradation, while the other component binds to an E3 ubiquitin ligase or other effector of cellular degradation.[46] The induced proximity of target protein to the E3 ligase allows the E3 ligase to ubiquitinate the target protein. Once ubiquitinated, the target protein can be recognized by the proteasome and

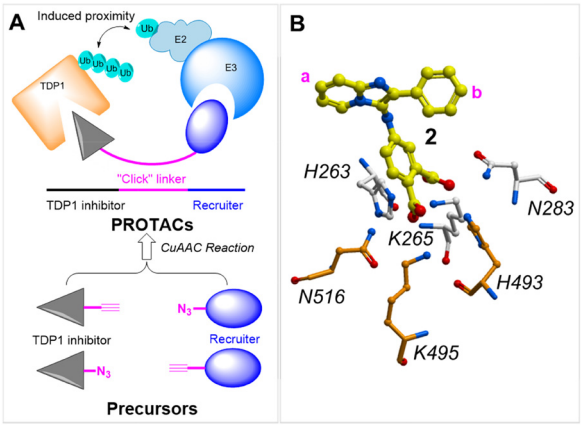

Fig. 2 PROTAC structural schematic and the binding interactions of an imidazopyridine TDP1 inhibitor. (A) PROTAC induced proximity and preparation using click chemistry. TDP1 inhibitor (grey triangle) linked with recruiter (blue oral) leads to induced proximity between TDP1 and an E3 ligase that leads to enhanced ubiquitination of TDP1. (B) Crystal structure of TDP1-bound imidazopyridine inhibitor **2** (carbon atoms are shown in yellow) binding at the catalytic site. The catalytic residues of the HKN motifs are shown in grey and orange (PDB code: 6W7K). Positions on inhibitor **2** labeled "a" and "b" point toward the solution phase serve as potential sites to introduce linkers attached to E3 recruiting functionality.

degraded into smaller peptides. This process effectively reduces the cellular levels of the target protein, representing an alternative to traditional down-regulation of function by small molecule inhibitors. PROTACs are a relatively new class of therapeutic molecules designed to selectively modulate protein function by inducing ubiquitination and degrading cellular target proteins (Fig. 2A).[47–49] Protein degraders have potential advantages over other small-molecule inhibitors used for cancer treatment.[50] Unlike traditional small molecules that inhibit protein function, PROTACs harness the cellular ubiquitin–proteasome system to tag the target protein for degradation. They can potentially lead to more complete and durable therapeutic effects with higher selectivity as compared to classic enzymic inhibitors. The chemical biology toolbox for studying TDP1 could be significantly enhanced by having ability to selectively reduce the levels of TDP1 using protein degraders. Such agents could potentially synergize with current TOP1 inhibitors and enhance potency and selectivity. The focus of our current work is to explore synthetic approaches to modifying known TDP1 inhibitors in ways that permit installation of E3 ligase-targeting functionality, while maintaining the ability of the ligands to retain the ability to bind to TDP1.

Results and discussion

Enzyme degradation represents a new approach to address problems faced in developing TDP1 inhibitors

Members of the PROTAC class of molecular degraders typically have three key components: (A) a ligand that binds to the protein being targeted for degradation; (B) a E3 ligase-binding motif and (C) suitable linker functionality that joins

these two components (Fig. 2A). E3 ubiquitin ligases are protein complexes that covalently modify other proteins with ubiquitin. Once tagged with ubiquitin, the target protein is recognized by the proteasome for degradation. Following ubiquitination, the PROTAC molecule can dissociate to target additional proteins. Highly efficient PROTACs could be very powerful tools in chemical biology and represent potential platforms for drug discovery.[51]

The von Hippel–Lindau (VHL) and cereblon (CRBN) E3 ubiquitin ligases are extensively used for PROTAC design.[46] VHL-containing E3 ubiquitin ligase complexes target proteins for degradation, particularly under low oxygen conditions. Hydroxyproline-containing small molecules can mimic the hydroxyproline residues found in the cognate VHL-binding domain of hypoxia-inducible factor (HIF-α). Appending these motifs to ligands can facilitate the targeted degradation normally induced by HIF-α. The E3 ubiquitin ligase CRBN plays a critical role in protein degradation by recruiting immunomodulatory drugs (IMiDs), such as thalidomide and its derivatives lenalidomide and pomalidomide. These IMiDs bind to CRBN and promote the degradation of specific substrates.

In the process of ubiquitination, lysine residues on the target protein serve as crucial anchor roles in the formation of the polyubiquitin chains that are essential for marking the protein for degradation. TDP1 contains a total of 52 lysine residues and many of them may potentially be positioned to serve as anchors for ubiquitination (Fig. 1C). Linkers joining the target protein and E3 ligase binding components are key factors in determining their efficacy, specificity, and overall performance of PROTACs.[52] The length and flexibility of the linker can significantly influence the binding efficiency and the orientation of the two components. The linkers can provide the necessary conformational freedom for the PROTAC to adopt an optimal shape for engaging both the target protein and the E3 ligase. This is essential for effective ubiquitination and subsequent degradation. Fine-tuning the linker can improve the selectivity for the target protein, reduce off-target effects and enhance overall efficacy. Linkers can also influence the stability and solubility of PROTACs. A balanced linker design helps ensure that the compound remains stable in biological environments and maintains adequate solubility for cellular uptake, which improve the overall drug-like properties of the molecule.[53]

Design of bivalent TDP1 PROTACs based on insights derived from the X-ray cocrystal structures of TDP1 inhibitors bound at the catalytic site

We previously employed a crystallographic fragment cocktail screen of more than 600 small molecule fragments to discover phthalic acids and quinolones that bind within the TDP1 catalytic hot spot.[20] Recently, we also combined small molecule microarray (SMM) and oxime diversification strategies to develop more extended ligands (**1**–**3**) intended to engage residues within the catalytic pocket, while extending into the DNA and peptide-binding channels (Fig. 1A).[20,22,24] Certain of these constructs showed micromolar inhibitory values in *in vitro* assays. However, inhibitory efficacies in whole cell systems were less than what would be expected based on the results from the *in vitro* assays. Crystal structures of the lead compounds, such as phenyl imidazopyridine **2** (Fig. 1A), showed that the phthalic acid component replicate aspects of substrate phosphates by forming several direct hydrogen bonds with the key catalytic residues (Fig. 1B and 2B).[22] In further work, we used oxime diversification strategies to develop a series of analogues having R^a or R^b substituents at the pyridine or phenyl rings (**3**, Fig. 1A).[22,24]

The structural complexity and dynamics of degradation complexes render it challenging to predict which combination of anchor-linker-warhead will lead to optimal degradation. The linkers play particularly crucial roles in the design and function of PROTACs. A diverse range of linkers have been applied to design PROTACs. These include polyethylene glycol (PEG) and alkyl chains, and chains containing glycol, alkyne, triazole, piperazine, and piperidine components.[52] Based on the binding mode of our phenyl imidazopyridine-based TDP1 inhibitors as revealed in ligand-bound crystal structures (Fig. 1B and 2B), we designed a series of TDP1 PROTACs **4** and **5** with linkers of varying lengths (Fig. 2A and 3). The TDP1 PROTACs **4** and **5**

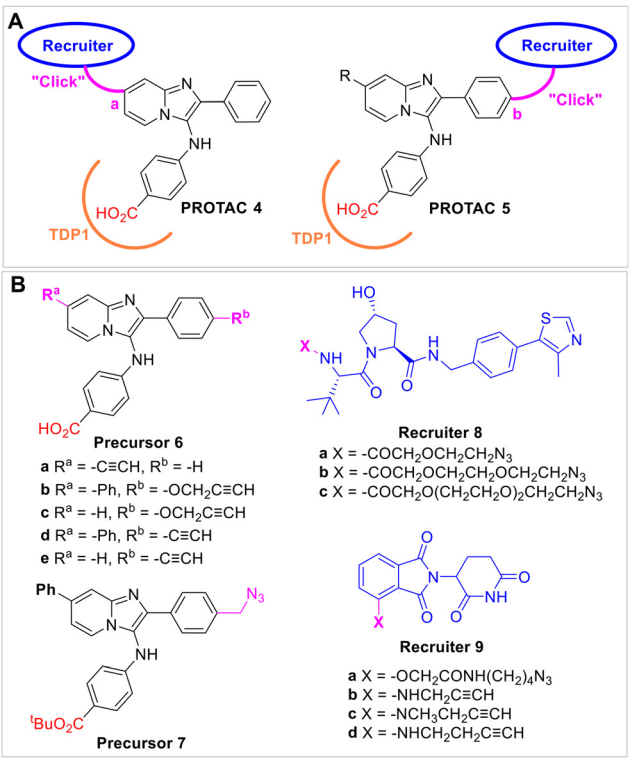

Fig. 3 Design of TDP1 PROTACs that employ alkyne and azide precursors. (A) Structures of PROTACs (**4** and **5**) that append the recruiter linkers at the pyridine ring site "a" and the phenyl ring site "b" positions, respectively. (B) Structures of "click" functionality-bearing intermediates; phenyl imidazopyridine-derived TDP1-binding analogs (**6a**–**6e** and **7**); and VHL-recruiter hydroxyproline-derived precursors (**8a**–**8c**) and CRBN-recruiter thalidomide-derived precursors (**9a**–**9d**).

incorporate VHL recruiters and CRBN recruiters on either side of the phenyl imidazopyridine-based TDP1 catalytic pocket-binding core. Placement of E3-recruiting functionality was designed to situate linkers pointing away from the TDP1 protein and toward the solution phase.

"Click chemistry" is widely used, particularly in expediting drug discovery and optimization processes. It has also been used to conjugate linkers and components in the synthesis of PROTACs.[54,55] In our current work, we employed Huisgen copper-catalyzed azide–alkyne cycloaddition (CuAAC) click chemistry to couple azides and terminal alkynes to give 1,2,3-triazoles. The triazole groups in the resulting TDP1 inhibitors were formed from alkyne-labeled phenyl imidazopyridine precursors **6a–6e** and azide-labeled phenyl imidazopyridine precursor **7** as well as the azide-labeled VHL-recruiter precursors **8a–8c**, the azide-labeled CRBN-recruiter precursor **9a** and the alkyne-labeled CRBN-recruiter precursors **9b–9d**. We are not aware of prior reports detailing TDP1-targeting PROTACs.

Synthesis

We have previously prepared TDP1 inhibitors that contain triazole moieties as isosteric replacements of our lead oxime-based TDP1 inhibitors.[24] The syntheses of these compounds employed key one-pot Groebke–Blackburn–Bienaymé multicomponent reactions (GBBR) together with copper-catalyzed azide–alkyne cycloaddition (CuAAC) click chemistry.[24] As shown in Scheme 1, we used this chemistry to prepared alkyne-labeled precursor **6a**. Starting from the 4-ethynylpyridin-2-amine **10**, benzaldehyde **11** and methyl 4-isocyanobenzoate **12**, we prepared ester **13** having alkyne functionality on the pyridine ring. Hydrolysis of **13** using sodium hydroxide in methanol afforded the alkyne-labeled acid precursor **6a**. Click coupling of alkyne **6a** with commercially available azide-labeled VHL recruiters **8a–8c** having different length glycol linkers, yielded final bivalent analogs **4a–4c**. Analogue **4d** was prepared from alkyne **6a** and commercially available alkyne-labeled CRBN-recruiter **9a** using the same CuAAC click reaction catalyzed by tris((1-benzyl-4-triazolyl)methyl)amine (TBTA) (Scheme 1).

We have previously reported the preparation of alkyne-labeled phenyl imidazopyridine analogues **6b–6e** using GBBR reactions.[24] As shown in Scheme 2, the alkyne-labeled phenyl imidazopyridine analogues **6b–6e** were easily coupled with the azide-labeled VHL recruiters **8a–8c** and the alkyne-labeled CRBN-recruiter **9a** to afford bivalent analogs **5a–5g**.

Methyl ester hydrolysis to the corresponding carboxylic acids using sodium hydroxide in methanol was not compatible with the imide functionality in CRBN-recruiter thalidomide derivatives and precursors. Therefore, we changed the protection groups from methyl esters to *tert*-butyl esters. As shown in Scheme 3, we prepared *tert*-butyl ester **17** using the GBBR reaction of 4-phenylpyridin-2-amine **14**, 4-(hydroxymethyl)benzaldehyde **15**, and *tert*-butyl 4-isocyanobenzoate **16**. Application of the Appel reaction using tetrabromide carbon and triphenylphosphine in acetonitrile converted the hydroxyl in **17** to afford bromide **18**.[56] This was followed by displacement of the bromide using sodium azide in acetone to yield azide-labeled precursor **7**. The alkyne-labeled pomalidomides **9b–9d** were prepared by SNAr reactions of fluoride **19** with a variety of amine-containing alkynes that included prop-2-yn-1-amine, *N*-methylprop-2-yn-1-amine or but-3-yn-1-amine.[57] CuAAC coupling of azide-labeled precursor **7** and alkyne-labeled pomalidomides **9b–9d** afforded **20a–20c**. Deprotection of the acid-labile *tert*-butyl groups in **20a–20c** using TFA provided the final bivalent analogs **5h–5j** (Scheme 3).

Inhibition of TDP1 in gel-based fluorescence assays

We evaluated the *in vitro* TDP1 inhibitory potencies of triazole-linked PROTAC conjugates **4a–4d** and **5a–5j** using gel-based fluorescence assay with TDP1 (Tables 1 and S1, ESI†). We previously reported that the parent compound **1a** shows single-digital micromolar inhibitory potency *in vitro* (**1a**,TDP1 IC_{50} = 8.72 ± 1.81 μM).[22,24] As shown in Table 1, addition of different length PEG-linked hydroxyproline-containing VHL recruiters at the "a" position of compound

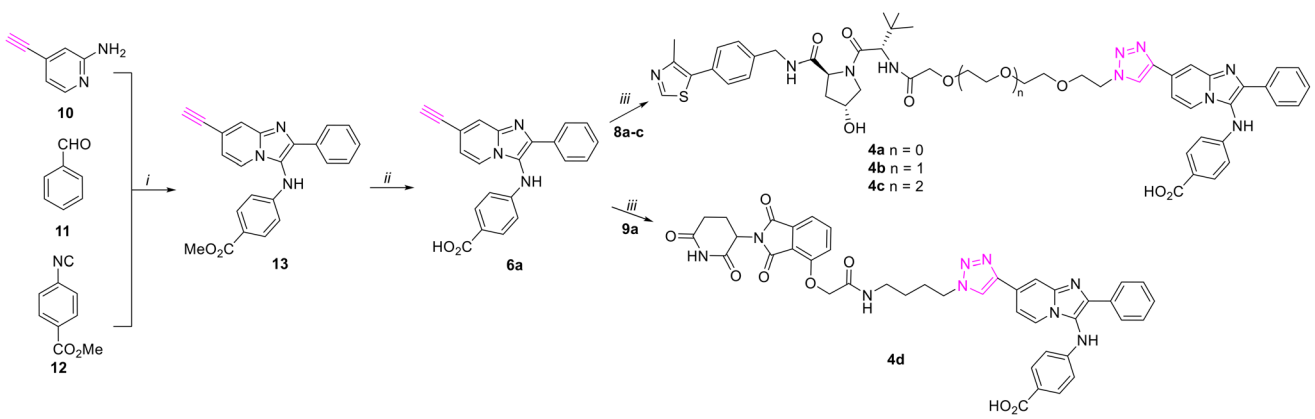

Scheme 1 Synthesis of compounds **4a–4d** using key GBBR multi-component reaction and CuAAC "click" reaction. Reagents and conditions: (i) HOAc, MeOH; (ii) NaOH, MeOH; (iii) TBTA, $CuSO_4$–$5H_2O$, sodium L-ascorbate, DMSO, H_2O, rt.

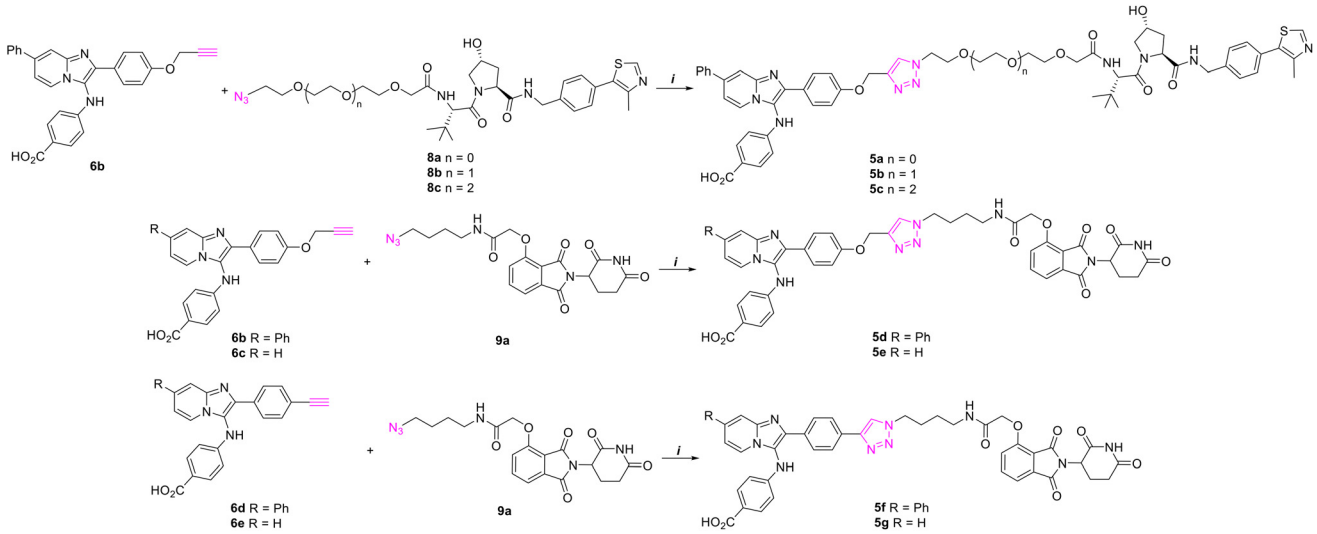

Scheme 2 Synthesis of compounds **5a–5g** using CuAAC click reaction. Reagents and conditions: (i) TBTA, $CuSO_4$–$5H_2O$, sodium L-ascorbate, DMSO, H_2O, rt.

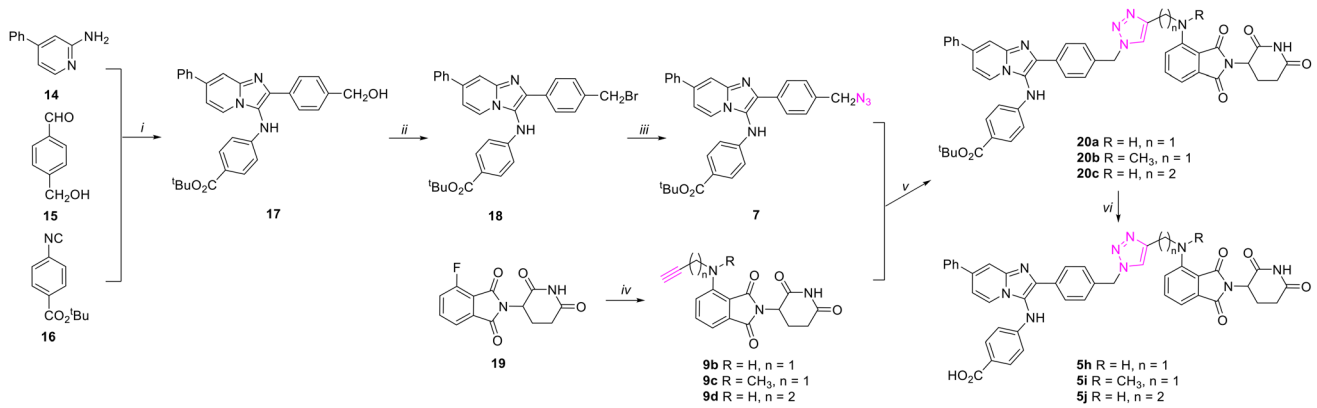

Scheme 3 Synthesis of compounds **5h–5j** using key GBBR multi-component reaction and CuAAC "click" reaction. Reagents and conditions: (i) HOAc, MeOH; (ii) CBr_4, Ph_3P, CH_3CN, rt; (iii) NaN_3, CH_3COCH_3, 55 °C; (iv) amines (**a**, $CH{\equiv}CCH_2NH_2$; **b**, $CH{\equiv}CCH_2NHCH_3$; **c**, $CH{\equiv}CCH_2CH_2NH_2$), DMSO, 130 °C; (v) TBTA, $CuSO_4$–$5H_2O$, sodium L-ascorbate, DMSO, H_2O, rt. (vi) TFA, DCM.

1a, gave conjugates **4a–4c**, which fail to show TDP1 inhibitory potencies (**4a–4c**, TDP1 $IC_{50} > 100$ μM). Addition of alkyl-linked thalidomide CRBN recruiters at the "a" position of **1a** gave conjugate **4d**, which also failed to show inhibitory potency within the tested range (**4d**, TDP1 $IC_{50} > 100$ μM). Parent compound **1b** with a phenyl at "a" position of **1a** shows slightly better TDP1 inhibitory potency than **1a**.[22,24] We moved the PEG-linked hydroxyproline-containing VHL recruiters in conjugates **4a–4c** to the "b" position of compound **1b** to yield compounds **5a–5c**. Although the resulting conjugates **5b** and **5c** still failed to exhibit TDP1 inhibitory potency within the range tested, conjugate **5a** having the shortest PEG linker showed moderate inhibitory potency (**5a**, TDP1 IC_{50} = 70.3 ± 2.4 μM, Table 1). Next, we replaced the PEG-linked hydroxyproline-containing VHL moieties to alkyl-linked CRBN-binding fragments to yield **5d–5g**. Although conjugates **5d**, **5e** and **5g** did not show TDP1 inhibitory potency within the range tested, the inhibitory potency of conjugate **5f** (TDP1 IC_{50} = 33.1 ± 7.2 μM) was greater than **5a** (Table 1). These results suggest that the best combination of features would be to use the CRBN warhead (as for **5f**) along with shorter length linkers (as seen with **5a**) attached at the "b" position of **1b**. Based on this, we prepared the conjugates **5h–5j** having shorter triazole-linked pomalidomide CRBN-targeting functionality. Conjugates **5h–5j** showed better TDP1 inhibitory potency than both **5a** and **5f** (**5h**, TDP1 IC_{50} = 7.41 ± 0.19 μM; **5i**, TDP1 IC_{50} = 18.5 ± 1.55 μM; **5j**, TDP1 IC_{50} = 12.34 ± 1.5 μM, Table 1). Encouragingly, conjugate **5h** displayed an IC_{50} values against TDP1 that was comparable to the parent compounds **1a** and **1b** (**5h**, TDP1 IC_{50} = 7.41 ± 0.19 μM *vs.* **1a**, TDP1 IC_{50} = 8.72 ± 1.81 μM and **1b**, TDP1 IC_{50} = 2.98 ± 0.24 μM).

Unless indicated otherwise, we conducted the gel-based fluorescence assay using full-length TDP1 (Table 1).[22,24] However, in our SMM screen and crystallography studies we used truncated TDP1(148–608), which contains the catalytic

Table 1 TDP1 inhibitory potencies of bivalent analogs determined in an *in vitro* gel-based fluorescence assay[a]

Compound	TDP1 IC_{50} (μM)
1a	8.72 ± 1.81[b]
1b	2.98 ± 0.24[b]
4a	>100
4b	>100
4c	>100
4d	>100
5a	70.3 ± 2.4
5b	>100
5c	>100
5d	>100
5e	>100
5f	33.1 ± 7.2
5g	>100
5h	7.41 ± 0.19
5i	18.5 ± 1.55
5j	12.34 ± 1.5
1b [TDP1(148–608)]	6.6×[c]
5h [TDP1(148–608)]	1.2×[c]

[a] The half maximal inhibitory concentration (IC_{50}) based on gel-based TDP1 fluorescence assay. Except where indicated, assays were conducted using full-length TDP1. [b] IC_{50} values have been reported previously.[22,24] [c] Fold-loss of IC_{50} values against truncated TDP1(148–608) *vs.* wild-type TDP1.

domain but lacks the N-terminal flexible domain (residues 1–147).[22,24] The N-terminal domain has been shown to play important roles in the cellular actions of TDP1 (ref. 58) and this domain has also been shown to be critical for allosteric inhibition by the recently discovered macrocyclic peptide.[42] Although the structure of full-length TDP1 has remained elusive, its presence can significantly impact the function of TDP1. We evaluated **5h** and **1b** against truncated TDP1(148–608). Parent compound **1b** showed 6.6-fold lower IC_{50} values against truncated TDP1(148–608) as compared with against wild-type full-length TDP1 (Table 1). This suggests a potential role for the N-terminal domain in the action of **1b**. However, conjugate **5h** showed a more modest 1.2-fold reduction in IC_{50} value against truncated TDP1(148–608) as compared with wild-type full-length TDP1 (Table 1). This indicates that **5h** can retain binding to TDP1 catalytic domain even without the N-terminal flexible loop. This data suggests that conjugate **5h** could have greater tolerance for changes in the TDP1 tertiary structure.

Comparison of TDP1 inhibitory potencies with TDP2 inhibitory potencies

TDP2 is a structurally different tyrosyl-DNA phosphodiesterase enzyme involved in the repair of TOP2ccs and TOP3ccs.[10,17,59,60] TDP1 and TDP2 were discovered and named based on the fact they process 3′- and 5′-DNA ends by excising irreversible protein tyrosyl-DNA complexes involving topoisomerases I and II, respectively.[6] Both enzymes have an extended spectrum of activities. Human TDP2 is smaller than TDP1 with a molecular mass of 41 kDa (362 amino acid residues). The repair function of TDP2 is devoted to the excision of topoisomerase II- and potentially topoisomerases III-DNA adducts. Like TDP1, TDP2 is a two-domain protein with the catalytic domain in the C-terminus and an N-terminal domain that is thought to play a regulatory role. Unlike TDP1, TDP2 catalysis requires divalent metals but does not form a transient covalent catalytic intermediate.

As a counter screen to the *in vitro* TDP1 assay, we determined the inhibitory potencies of compounds **1a**, **1b**, **5a**, **5f**, **5h–5j** against full-length TDP2 in gel-based *in vitro* fluorescence assays and compared these values with full-length TDP1 inhibitory potencies (Table 2). Parent compounds **1a** and **1b** showed single-digital micromolar TDP1 inhibitory potencies but failed to inhibit TDP2 within the maximum assay concentration of 100 μM (Table 2). However, the lead conjugates **5a**, **5f**, and **5h–5j** showed only slightly reductions in inhibitory potencies against TDP2 as compared with against TDP1. Since conjugates **5f** and **5h–5j** showed micromolar inhibitory potencies against both TDP1 and TDP2 *in vitro*, this may potentially suggest that promiscuous inhibition may be at work.[44]

The bivalent analogs do not appear to get into cells

In cellular assays, compound **5h** failed to show significant cytotoxicity when used as single agents (CC_{50} ~193 μM in HCT116 cell line, Table S2, ESI†). We were unable to observe degradation effects of **5h** and **5i** in the HCT116 cell line compared with reference glyceraldehyde 3-phosphate dehydrogenase (GAPDH) (Fig. 4A and B). Compound **5h** also failed to show synergy when used in combination with the TOP1 inhibitor camptothecin (CPT) in either HCT116 or U2OS cell lines (Fig. 4C). We interpreted this to mean that the compounds did not get into cells. Even though both of warhead components bind well to the target proteins, the absence of

Table 2 TDP1 selectivity of lead compounds compared with TDP2 using gel-based assays *in vitro*

Compound	TDP1 IC_{50}[a] (μM)	TDP2 IC_{50}[b] (μM)	TDP1 selectivity[c]
1a	8.72 ± 1.81	>100	>11
1b	2.98 ± 0.24	>100	>33
5a	70.3 ± 2.4	>100	1.4
5f	33.1 ± 7.2	37.3 ± 4.5	1.1
5h	7.41 ± 0.19	11.2 ± 0.55	1.5
5i	18.5 ± 1.55	21.2 ± 0.15	1.1
5j	12.34 ± 1.5	16.8 ± 0.3	1.4

[a] Half maximal inhibitory concentration (IC_{50}) based on gel-based TDP1 fluorescence assay. [b] Half maximal inhibitory concentration (IC_{50}) based on gel-based TDP2 fluorescence assay. [c] TDP1 selectivity based on the ratio of IC_{50} values of TDP2 *vs.* TDP1.

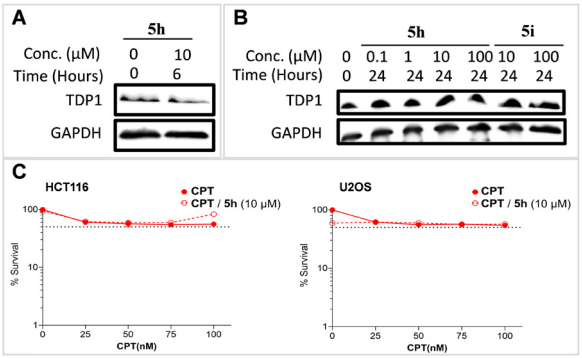

Fig. 4 TDP1 degradation and synergy result of compound **5h**. (A) TDP1 degradation of compound **5h** at 10 μM compared with GAPDH within 6 hours in the HCT116 cell line. (B) TDP1 gel bands of compound **5h** at 0.1, 1, 10, 100 μM and **5i** at 10, 100 μM separately compared with GAPDH within 24 hours in TDP1 degradation in the HCT116 cell line. (C) Synergy curves of compound **5h** at 10 μM with TOP1 inhibitor CPT in HCT116 and U2OS cell lines separately.

cellular activity is most reasonably explained by lack of cell penetration.[51] PROTACs are often affected by poor cellular permeability due to their high molecular weight and large exposed polar surface area.[61] This is a common challenge presented by PROTACs.

PROTAC modeling

PROTACs induce ternary complexes that lead to ubiquitination and degradation of target proteins. A variety of methodologies have been employed to generate ternary structure of E3-PROTAC-target complexes.[62] In our current work we linked lead imidazopyridine TDP1 inhibitor (**1b**) together with thalidomide (**21**) using triazole-forming "click" chemistry to provide bivalent conjugate (**5h**) as putative PROTAC analog (Fig. 5A). We endeavored to employ *in silico* modeling to explore potential geometries of PROTAC-induced proximity positioning of TDP1 with an E3 ligase. We start from the structures of the DDB1-CRBN (DNA damage-binding protein 1-cereblon) E3 ubiquitin ligase in complex with thalidomide (**21**, PDB code: 4CI1)[63] and TDP1 bound with imidazopyridine inhibitor (**2**, PDB code: 6W7K).[22] Using our ICM MolSoft Pro 64 (icm 3.9–4) software,[64] we formed the ternary structure of E3-TDP1 complexes bound to lead conjugate **5h**. We employed the following protocol: (1) read into ICM the target PDB files for TDP1 "6W7K" and CRBN "4CI1" (Fig. 5B and C); (2) delete portions of ligand structures not needed and convert both assemblies into ICM objects; (3) read in a .sdf file of molecule **5h** in chemical table; (4) run PROTAC Modeling using protein–protein docking PROTAC model builder in ICM module. This provided a model of the PROTAC complex having the conjugate **5h** bound to the CRBN (shown in cyan ribbon) and TDP1 (shown in grey ribbon) with the triazole linker bridging the imidazopyridine TDP1 inhibitor and thalidomide (Fig. 5D and E). This suggests that the PROTAC conjugate **5h** could reasonably induce spatial proximity of both TDP1 and CRBN (Fig. 5F and G). The linker of compound **5h** locates at the peptide binding groove side, points toward the opposite of the TDP1 catalytic site and extends to the CRBN binding site, which is what we excepted.

Conclusions

The development of clinical TDP1 inhibitors has been highly challenging. The chemical biology toolbox for studying TDP1 could be significantly enhanced by including the ability to selectively degrade TDP1 using protein degraders. Guided by the crystal structures of TDP1 bound to phenyl imidazopyridine (**2**), we designed a series of bivalent constructs with different length linkers (**4a–4d** and **5a–5j**) that were intended to function as TDP1 PROTACs. These TDP1 PROTACs employ E3 ligase-targeting components VHL recruiter and CRBN recruiter linked to both sides of the phenyl imidazopyridine-based TDP1-binding core. We prepared these from azide and alkyne precursors using straightforward CuAAC click chemistry. The primary objective of our current work has been to explore synthetic approaches to modifying known TDP1 inhibitors in ways that would permit installation of E3 ligase-targeting functionality, while retaining the ability of the ligands to bind to TDP1. We found among the conjugates **5h–5j** that shorter linkers retain micromolar inhibition against TDP1 in gel-based fluorescence assays *in vitro*. Conjugate **5h** shows single-digital micromolar TDP1 inhibitory potency. In cellular assays, these bivalent constructs fail to show biological activity. We interpret this to indicate extremely poor cellular uptake. None-the-less, our work validates approaches to designing and synthesizing bivalent ligands having key molecular features needed for functional TDP1 PROTACs. These results should enrich to chemical biology toolbox for studying TDP1 function.

Materials and methods

TDP1 and TDP2 gel-based assay *in vitro*

The inhibition assays for full-length TDP1, N-terminally truncated TDP1(148–608) and TDP2 were performed following previously described gel-based methods.[22,24,43] Briefly, 1 nM of the DNA substrate (N14Y, 5′Cy5-GATCTAAAAGACTT-pY-3′) was incubated with 40 pM full-length recombinant TDP1 or truncated TDP1(148–608) in the absence or presence of inhibitors for 15 min at room temperature (rt) in TDP1 reaction buffer (50 mM Tris-HCl, pH 7.5, 80 mM KCl, 2 mM EDTA, 1 mM DTT, 40 μg mL^{-1} BSA and 0.01% Tween 20). Similarly, 1 nM of DNA substrate (YN18, 5′-pY-TCCGTTGAAGCCTGCTTT-Cy5-3′) was incubated with 40 pM recombinant TDP2 under identical conditions, except using TDP2 reaction buffer (50 mM Tris-HCl, pH 7.5, 80 mM KCl, 5 mM $MgCl_2$, 0.1 mM EDTA, 1 mM DTT, 40 μg mL^{-1} BSA, and 0.01% Tween 20). The reactions were stopped by adding an equal volume of gel loading buffer (99.5% (v/v) formamide, 5 mM EDTA). The samples were then subjected to a 20% denaturing PAGE gel followed by gel scanning using a Typhoon FLA 9500 scanner (GE Healthcare). The IC_{50} values of the TDP1 inhibitors were calculated by

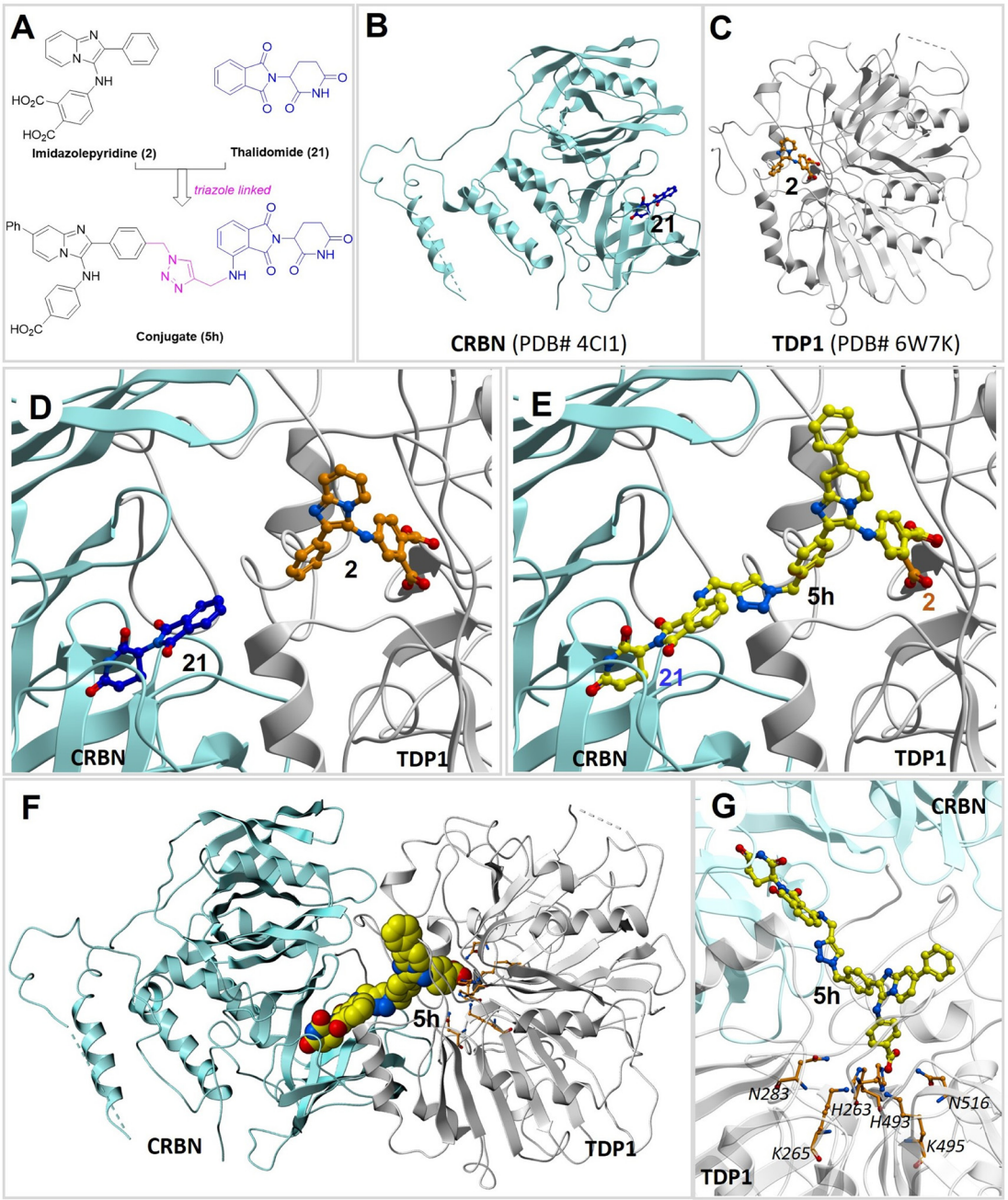

Fig. 5 Docking modes of conjugate **5h** with TDP1 and CRBN. (A) Structures of lead imidazopyridine TDP1 inhibitor **2**, thalidomide **21** and conjugate **5h**. (B) Crystal structure of CRBN (shown in cyan ribbon) bound with thalidomide **21** (shown in blue carbons) (PDB code: 4CI1). (C) Crystal structure of TDP1 (shown in grey ribbon) bound with imidazopyridine TDP1 inhibitor **2** (shown in brown carbons) (PDB code: 6W7K). (D) Close view of thalidomide **21** and imidazopyridine TDP1 inhibitor **2** (shown in brown carbons) binding at the interface of CRBN and TDP1 enzymes. (E) Overlaid mode of conjugate **5h** with thalidomide **21** and imidazopyridine TDP1 inhibitor **2** at the interface of CRBN and TDP1 enzymes. (F) Binding mode of conjugate **5h** (carbons are shown in yellow spheres) at the interface of CRBN enzyme (shown in cyan ribbon) and TDP1 enzyme (shown in grey ribbon). (G) Binding mode of conjugate **5h** (carbons are shown in yellow balls) at the interface of CRBN enzyme (shown in cyan ribbon) and TDP1 enzyme (shown in grey ribbon).

comparing the percentage of the cleavage product (N14P, 5′Cy5-GATCTAAAAGACTT-p-3′) produced to that in the DMSO control. The IC_{50} values of the TDP2 inhibitors were calculated by comparing the percentage of the cleavage product (PN18, 5′-p-TCCGTTGAAGCCTGCTTT-Cy5-3′) produced to that in the DMSO control.

Survival curve and cytotoxicity[24]

MCF7 or HCT116 cells were seeded into 384-well black-clear plate until 30% confluency and then incubated with a two-fold serial dilution of TDP1 inhibitors for 72 h at 37 °C (Table S2, ESI†). The cell numbers were counted from the brightfield

images taken by Biotek Cytation 5. The cell cytotoxicity was calculated based on the concentration required for 50% cell survival (CC_{50}), using DMSO as a control.

Synergy assay of TDP1 inhibitors with camptothecin (CPT)

The synergistic effects of the TDP1 inhibitors with CPT were tested in the human colon cancer HCT116 cell line and osteosarcoma U2OS cell line based on cell viability.[22,24,43] Cells were first seeded into 384-well opaque plate at a density of 2×10^3 cells per well and then were cultured for 72 hours in a media containing the drugs. Cell viability was assessed by using CellTiter-Glo Luminescent Cell Viability Assay (Promega, no. G7570) according to the manufacturer's instructions and luminescence intensity was measured using SpectroMaxi3, CellTiter-Glo cell proliferation program.

Western blot for TDP1 degradation

Cells treated with or without inhibitors were lysed in 100 μL sodium dodecyl sulfate (SDS) buffer containing 25 mM Tris-HCl (pH 6.5), 1% SDS, 0.24 mM β-mercaptoethanol, 0.1% bromophenol blue and 5% glycerol and cOmplete™, Mini, EDTA-free protease inhibitor cocktail (Roche, Cat# 11836170001). Whole-cell extracts were separated by SDS-PAGE gel, transferred onto polyvinylidene difluoride (PVDF) membranes, and blocked in 5% skimmed milk dissolved in 0.1% Tween-20 in phosphate buffer saline (PBS). Membranes were incubated with primary antibodies overnight at 4 °C followed by washing with 0.1% Tween-20 in PBS. Primary antibodies used in this study are as follows: rabbit polyclonal anti-TDP1 (dilution 1 : 1000, ABCAM, Cat# ab227144) and rabbit mAb anti-GAPDH (dilution 1 : 2000, Cell Signaling Technology, Cat# 2118, Clone 14C10). Membranes were incubated with anti-rabbit IgG ECL, HRP conjugated (dilution 1 : 4000, GE Healthcare, Cat# NA9340) at rt for 1 h and washed thrice and signals were detected by ECL chemiluminescence reaction (SuperSignal™ West Femto Maximum Sensitivity Substrate, Thermo Scientific, Waltham, MA, Cat# 34095).

General procedures

Proton (^{1}H) and carbon (^{13}C) NMR spectra were recorded on a Varian 400 MHz spectrometer or a Varian 500 MHz spectrometer and are reported in ppm relative to TMS and referenced to the solvent in which the spectra were collected. Solvent was removed by rotary evaporation under reduced pressure, and anhydrous solvents were obtained commercially and used without further drying. Purification by silica gel chromatography was performed using Combiflash with EtOAc–hexanes solvent systems. Preparative high pressure liquid chromatography (HPLC) was conducted using a Waters Prep quaternary gradient module 2535 system having photodiode array detector 2998, fraction collector III, autosampler 2707 and Phenomenex C18 columns (catalogue no. 00G-4436-P0-AX, 250 mm × 21.2 mm 10 μm particle size, 110 Å pore) at a flow rate of 10 mL min^{-1} or 20 mL min^{-1}. Binary solvent systems consisting of A = 0.1% aqueous TFA and B = 0.1% TFA in acetonitrile were employed with gradients as indicated. Products were obtained as amorphous solids following lyophilization. Electrospray ionization-mass spectrometric (ESI-MS) were acquired with an Agilent LC/MSD system equipped with a multimode ion source. High resolution mass spectrometric (HRMS) were acquired by LC/MS-ESI using LTQ-Orbitrap-XL at 30 K resolution.

General procedure A. Use of CuAAC to prepare triazole PROTACs (4a–4d, 5a–5g, and 20a–20c)[65]. Alkynes (**6a–6e** or **9b–9d**, 0.1 mmol, 1 mg in 10 μL DMSO), azides (**8a–8c**, **9a** or **7**, 0.1 mmol, 1 mg in 10 μL DMSO) and tris((1-benzyl-1*H*-1,2,3-triazol-4-yl)methyl)amine (TBTA, 0.04 mmol, 1 mg in 10 μL DMSO) were mixed in a vial with a stirrer bar. Sodium L-ascorbate (0.1 mmol, 1 mg in 10 μL H_2O) and $CuSO_4$–$5H_2O$ (0.02 mmol, 1 mg in 10 μL water) were added. The reaction was diluted in DMSO (2.0 mL). The formed bright yellow solution was stirred at rt overnight under argon. A yellow suspension was formed. The reaction mixture was dissolved in DMSO and purified by HPLC to afford triazole-containing conjugates (**4a–4d**, **5a–5g** and **20a–20c**).

General procedure B. Deprotection of *tert*-butyl group by TFA to prepare acids (5h–5j). Compound *tert*-butyl esters (**20a–20c**, 0.1 mmol) were mixed with TFA/DCM (1/1, 1.0 mL) at rt. The reaction mixture was stirred (rt, 30 min). The solvent was evaporated, and the residue was dissolved in MeOH and purified by preparative HPLC. The related fraction was collected and lyophilized to afford the related acids (**5h–5j**).

General procedure C. Preparation of alkyne-labeled pomalidomides (9b–9d)[57,66]. The commercially available 2-(2,6-dioxopiperidin-3-yl)-4-fluoroisoindoline-1,3-dione (**19**, 1.4 mmol), *N*-ethyl-*N*-isopropylpropan-2-amine (4.2 mmol) and alkyne amine (1.5 mmol) in DMSO (5.0 mL) was stirred (130 °C, 18 h). The reaction mixture was cooled to rt and purified by preparative HPLC. The related fraction was collected and lyophilized to afford the related alkynes (**9b–9d**).

Methyl 4-((7-ethynyl-2-phenylimidazo[1,2-*a*]pyridin-3-yl) amino)benzoate (13). The mixture of 4-ethynylpyridin-2-amine (**10**, 740 mg, 6.26 mmol), benzaldehyde (**11**, 0.7 mL, 6.89 mmol), acetic acid (0.7 mL, 12.53 mmol) was mixed in MeOH (10 mL) for 20 min. A brown solution was formed. Methyl 4-isocyanobenzoate (**12**, 1.1 g, 6.9 mmol)[22] was added. The formed brown solution was stirred at rt for 3 days. The final yellow suspension was filtered and washed by hexane. The pale-yellow solid was collected and afforded the title compound (**13**, 2.2 g, 5.9 mmol) as a pale yellow solid (95% yield). ^{1}H NMR (500 MHz, $CDCl_3$) δ 7.94–7.89 (m, 4H), 7.79 (s, 1H), 7.72 (dd, J = 7.0, 1.0 Hz, 1H), 7.37 (t, J = 7.4 Hz, 2H), 7.34–7.29 (m, 1H), 6.84 (dd, J = 7.0, 1.5 Hz, 1H), 6.59 (d, J = 8.4 Hz, 2H), 6.16 (s, 1H), 3.87 (s, 3H), 3.28 (s, 1H). ^{13}C NMR (126 MHz, $CDCl_3$) δ 166.87, 148.59, 142.01, 140.95, 132.51, 132.06 (2C), 128.76 (2C), 128.45, 127.04 (2C), 122.16, 121.91, 121.51, 119.17, 117.58, 115.33, 112.84 (2C), 81.81, 80.39, 51.87. ESI-MS m/z: 368.1 (MH^+).

4-((7-Ethynyl-2-phenylimidazo[1,2-*a*]pyridin-3-yl)amino)benzoic acid (6a). Sodium hydroxide (6.3 mL, 12.7 mmol) was added to

the solution of methyl 4-((7-ethynyl-2-phenylimidazo[1,2-*a*]pyridin-3-yl)amino)benzoate (**13**, 1.2 g, 3.2 mmol) in MeOH (8 mL) and THF (12 mL). The formed reddish-brown suspension was stirred at rt for 24 h. The suspension was acidified to form yellow suspension (pH ~8) by HCl (aq. 2N), Filtered and washed by water. The yellow solid was collected and purified by preparative HPLC (linear gradient of 20% B to 40% B over 20 min with a flow rate 20 mL min^{-1}; retention time = 12.3 min), the title compound (**6a**, 785 mg, 2.2 mmol) was afforded as a light-yellow solid (70% yield). ^{1}H NMR (400 MHz, DMSO-d_6) δ 12.35 (s, 1H), 8.90 (s, 1H), 8.02 (d, J = 7.2 Hz, 2H), 7.96 (d, J = 7.0 Hz, 1H), 7.84 (s, 1H), 7.77 (d, J = 8.4 Hz, 2H), 7.41 (t, J = 7.6 Hz, 2H), 7.31 (t, J = 7.3 Hz, 1H), 6.95 (dd, J = 7.0, 1.6 Hz, 1H), 6.58 (d, J = 8.2 Hz, 2H), 4.47 (s, 1H). ^{13}C NMR (126 MHz, DMSO-d_6) δ 167.59, 149.89, 141.57, 139.47, 133.48, 132.05 (2C), 129.07 (2C), 128.45, 126.94 (2C), 123.66, 121.28, 121.04, 119.18, 118.55, 115.17, 112.97 (2C), 83.95, 82.62. ESI-MS m/z: 354.1 (MH^+).

4-((7-(1-(2-(2-(2-(((*S*)-1-((2*S*,4*R*)-4-Hydroxy-2-((4-(4-methylthiazol-5-yl)benzyl)carbamoyl)pyrrolidin-1-yl)-3,3-dimethyl-1-oxobutan-2-yl)amino)-2-oxoethoxy)ethoxy)ethyl)-1*H*-1,2,3-triazol-4-yl)-2-phenylimidazo[1,2-*a*]pyridin-3-yl)amino)benzoic acid (4a). Treatment of 4-((7-ethynyl-2-phenylimidazo[1,2-*a*]pyridin-3-yl)amino)benzoic acid (**6a**) and commercially available (2*S*,4*R*)-1-((*S*)-2-(2-(2-(2-azidoethoxy)ethoxy)acetamido)-3,3-dimethylbutanoyl)-4-hydroxy-*N*-(4-(4-methylthiazol-5-yl)benzyl)pyrrolidine-2-carboxamide (**8a**) as outlined in general procedure A and purification by preparative HPLC (CAT# 00F-4436-U0-AX) (linear gradient of 25% B to 30% B over 20 min with a flow rate 20 mL min^{-1}, retention time = 15.6 min) provided the title compound (**4a**) as a white fluffy solid (34% yield).^{1}H NMR (500 MHz, DMSO-d_6) δ 12.42 (brs, 1H), 9.09 (s, 1H), 8.95 (s, 1H), 8.91 (s, 1H), 8.78 (d, J = 6.6 Hz, 1H), 8.30 (d, J = 7.3 Hz, 1H), 8.24 (t, J = 1.3 Hz, 1H), 7.93 (d, J = 7.1 Hz, 2H), 7.77 (d, J = 9.1 Hz, 2H), 7.73 (d, J = 7.7 Hz, 1H), 7.51 (t, J = 7.7 Hz, 2H), 7.43 (td, J = 8.7, 2.9 Hz, 2H), 7.37–7.32 (m, 4H), 6.73 (d, J = 8.1 Hz, 2H), 4.68–4.62 (m, 2H), 4.58 (d, J = 9.7 Hz, 1H), 4.50 (t, J = 8.3 Hz, 2H), 4.41–4.33 (m, 2H), 4.23 (dd, J = 15.8, 5.7 Hz, 2H), 3.96 (s, 2H), 3.94–3.90 (m, 2H), 3.66–3.57 (m, 5H), 2.40 (s, 3H), 2.10–2.05 (m, 1H), 1.92 (ddd, J = 13.0, 8.9, 4.5 Hz, 1H), 0.93 (s, 9H). ESI-MS m/z: 955.2 (MH^+). HRMS calcd for $C_{50}H_{55}N_{10}O_8S$ (MH^+), 955.3920; found, 955.3918. HRMS calcd. for $C_{50}H_{56}N_{10}O_8S$ $(MH_2)^{2+}$, 478.1996; found, 478.1990.

4-((7-(1-((*S*)-13-((2*S*,4*R*)-4-Hydroxy-2-((4-(4-methylthiazol-5-yl)benzyl)carbamoyl)pyrrolidine-1-carbonyl)-14,14-dimethyl-11-oxo-3,6,9-trioxa-12-azapentadecyl)-1*H*-1,2,3-triazol-4-yl)-2-phenylimidazo[1,2-*a*]pyridin-3-yl)amino)benzoic acid (4b). Treatment of 4-((7-ethynyl-2-phenylimidazo[1,2-*a*]pyridin-3-yl)amino)benzoic acid (**6a**) and commercially available (2*S*,4*R*)-1-((*S*)-14-azido-2-(*tert*-butyl)-4-oxo-6,9,12-trioxa-3-azatetradecanoyl)-4-hydroxy-*N*-(4-(4-methylthiazol-5-yl)benzyl)pyrrolidine-2-carboxamide (**8b**) as outlined in general procedure A and purification by preparative HPLC (CAT# 00F-4436-U0-AX) (linear gradient of 20% B to 35% B over 20 min with a flow rate 20 mL min^{-1}, retention time = 18.8 min) provided the title compound (**4b**) as a white fluffy solid (58% yield). ^{1}H NMR (500 MHz, DMSO-d_6) δ 12.42 (brs, 1H), 9.09 (s, 1H), 8.97 (s, 1H), 8.91 (s, 1H), 8.59 (t, J = 6.0 Hz, 1H), 8.34 (d, J = 7.0 Hz, 1H), 8.22 (s, 1H), 7.96–7.89 (m, 2H), 7.80–7.76 (m, 2H), 7.75 (d, J = 7.3 Hz, 1H), 7.52 (t, J = 7.6 Hz, 2H), 7.46–7.40 (m, 2H), 7.38 (s, 4H), 6.75 (d, J = 8.2 Hz, 2H), 4.62 (t, J = 5.2 Hz, 2H), 4.55 (d, J = 9.6 Hz, 1H), 4.43 (t, J = 8.2 Hz, 1H), 4.37 (s, 1H), 4.36–4.33 (m, 2H), 4.26 (d, J = 5.7 Hz, 1H), 4.23 (d, J = 5.7 Hz, 1H), 3.94 (s, 2H), 3.88 (t, J = 5.3 Hz, 2H), 3.65 (dd, J = 10.7, 3.9 Hz, 2H), 3.61–3.55 (m, 4H), 3.54 (td, J = 5.3, 2.5 Hz, 3H), 2.42 (s, 3H), 2.05 (ddd, J = 9.5, 7.7, 4.0 Hz, 1H), 1.89 (ddd, J = 13.0, 8.9, 4.5 Hz, 1H), 0.92 (s, 9H). ESI-MS m/z: 999.3 (MH^+). HRMS calcd. for $C_{52}H_{59}N_{10}O_9S$ (MH^+), 999.4182; found, 999.4167. HRMS calcd. for $C_{52}H_{60}N_{10}O_9S$ $(MH_2)^{2+}$, 500.2127; found, 500.2114.

4-((7-(1-((*S*)-16-((2*S*,4*R*)-4-Hydroxy-2-((4-(4-methylthiazol-5-yl)benzyl)carbamoyl)pyrrolidine-1-carbonyl)-17,17-dimethyl-14-oxo-3,6,9,12-tetraoxa-15-azaoctadecyl)-1*H*-1,2,3-triazol-4-yl)-2-phenylimidazo[1,2-*a*]pyridin-3-yl)amino)benzoic acid (4c). Treatment of 4-((7-ethynyl-2-phenylimidazo[1,2-*a*]pyridin-3-yl)amino)benzoic acid (**6a**) and commercially available (2*S*,4*R*)-1-((*S*)-17-azido-2-(*tert*-butyl)-4-oxo-6,9,12,15-tetraoxa-3-azaheptadecanoyl)-4-hydroxy-*N*-(4-(4-methylthiazol-5-yl)benzyl) pyrrolidine-2-carboxamide (**8c**) as outlined in general procedure A and purification by preparative HPLC (Cat# 00F-4436-U0-AX) (linear gradient of 20% B to 35% B over 20 min with a flow rate 20 mL min^{-1}, retention time = 19.2 min) provided the title compound (**4c**) as a white fluffy solid (61% yield). ^{1}H NMR (500 MHz, DMSO-d_6) δ 12.40 (brs, 1H), 9.03 (s, 1H), 8.97 (s, 1H), 8.88 (s, 1H), 8.60 (t, J = 6.1 Hz, 1H), 8.26 (s, 1H), 8.18 (s, 1H), 7.95 (d, J = 7.6 Hz, 2H), 7.80–7.74 (m, 2H), 7.67 (s, 1H), 7.48 (t, J = 7.6 Hz, 2H), 7.45–7.36 (m, 6H), 6.70 (s, 2H), 4.62 (t, J = 5.1 Hz, 2H), 4.55 (d, J = 9.7 Hz, 1H), 4.45–4.38 (m, 2H), 4.38–4.32 (m, 2H), 4.24 (dd, J = 15.8, 5.6 Hz, 1H), 3.94 (s, 2H), 3.88 (t, J = 5.2 Hz, 2H), 3.66 (dd, J = 10.7, 3.9 Hz, 2H), 3.59–3.55 (m, 3H), 3.55–3.51 (m, 4H), 3.51–3.46 (m, 5H), 2.43 (s, 3H), 2.06–2.02 (m, 1H), 1.89 (ddd, J = 13.1, 8.9, 4.5 Hz, 1H), 0.92 (s, 9H). ESI-MS m/z: 1143.2 (MH^+). HRMS calcd. for $C_{54}H_{63}N_{10}O_{10}S$ (MH^+), 1043.4444; found, 1043.4425. HRMS calcd. for $C_{54}H_{64}N_{10}O_{10}S$ $(MH_2)^{2+}$, 522.2258; found, 522.2243.

4-((7-(1-(4-(2-((2-(2,6-Dioxopiperidin-3-yl)-1,3-dioxoisoindolin-4-yl)oxy)acetamido)butyl)-1*H*-1,2,3-triazol-4-yl)-2-phenylimidazo[1,2-*a*]pyridin-3-yl)amino)benzoic acid (4d). Treatment of 4-((7-ethynyl-2-phenylimidazo[1,2-*a*]pyridin-3-yl)amino)benzoic acid (**6a**) and commercially available *N*-(4-azidobutyl)-2-((2-(2,6-dioxopiperidin-3-yl)-1,3-dioxoisoindolin-4-yl)oxy)acetamide (**9a**) as outlined in general procedure A and purification by preparative HPLC (Cat# 00F-4436-U0-AX) (linear gradient of 20% B to 40% B over 20 min with a flow rate 20 mL min^{-1}, retention time = 14.3 min) provided the title compound (**4d**) as a white solid (60% yield). ^{1}H NMR (500 MHz, DMSO-d_6) δ 12.43 (brs, 1H), 11.12 (s, 1H), 9.08 (s, 1H), 8.95 (s, 1H), 8.32 (d, J = 7.1 Hz, 1H), 8.19 (s, 1H), 8.05 (t, J = 5.8 Hz, 1H), 7.94 (d, J = 6.8 Hz, 2H), 7.82–7.76 (m, 3H), 7.72 (d, J = 7.1 Hz, 1H), 7.51 (t, J = 7.6 Hz, 2H), 7.47 (d, J = 7.2 Hz, 1H), 7.43 (t, J = 7.4 Hz, 1H), 7.38 (d, J = 8.5 Hz, 1H),

6.74 (d, J = 8.1 Hz, 2H), 5.11 (dd, J = 12.8, 5.4 Hz, 1H), 4.78 (s, 2H), 4.48 (t, J = 7.0 Hz, 2H), 3.21 (q, J = 6.6 Hz, 2H), 2.88 (ddd, J = 16.9, 13.8, 5.4 Hz, 1H), 2.64–2.52 (m, 2H), 2.03 (ddq, J = 10.6, 5.5, 2.5 Hz, 1H), 1.90 (p, J = 7.1 Hz, 2H), 1.47 (p, J = 7.0 Hz, 2H). ESI-MS m/z: 782.2 (MH^+). HRMS calcd. for $C_{41}H_{36}N_9O_8$ (MH^+), 782.2681; found, 782.2677.

4-((2-(4-((1-(2-(2-(2-(((*S*)-1-((2*S*,4*R*)-4-Hydroxy-2-((4-(4-methylthiazol-5-yl)benzyl)carbamoyl)pyrrolidin-1-yl)-3,3-dimethyl-1-oxobutan-2-yl)amino)-2-oxoethoxy)ethoxy)ethyl)-1*H*-1,2,3-triazol-4-yl)methoxy)phenyl)-7-phenylimidazo[1,2-*a*]pyridin-3-yl)amino)benzoic acid (5a). Treatment of 4-((7-phenyl-2-(4-(prop-2-yn-1-yloxy)phenyl)imidazo[1,2-*a*]pyridin-3-yl)amino)benzoic acid (**6b**)[24] and commercially available (2*S*,4*R*)-1-((*S*)-2-(2-(2-(2-azidoethoxy)ethoxy)acetamido)-3,3-dimethylbutanoyl)-4-hydroxy-*N*-(4-(4-methylthiazol-5-yl)benzyl) pyrrolidine-2-carboxamide (**8a**) as outlined in general procedure A and purification by preparative HPLC (CAT# 00F-4436-U0-AX) (linear gradient of 30% B to 35% B over 20 min with a flow rate 20 mL min^{-1}, retention time = 13.7 min) provided the title compound (**5a**) as a white fluffy solid (44% yield). ^{1}H NMR (500 MHz, DMSO-d_6) δ 12.43 (brs, 1H), 9.06 (s, 1H), 8.97 (s, 1H), 8.59 (t, J = 6.1 Hz, 1H), 8.31 (d, J = 7.0 Hz, 1H), 8.22 (s, 1H), 8.08 (d, J = 1.6 Hz, 1H), 7.93–7.85 (m, 4H), 7.82–7.74 (m, 2H), 7.66 (d, J = 6.6 Hz, 1H), 7.59 (dd, J = 8.3, 6.6 Hz, 2H), 7.56–7.51 (m, 1H), 7.45 (d, J = 9.7 Hz, 1H), 7.37 (s, 4H), 7.23–7.16 (m, 2H), 6.75 (d, J = 8.2 Hz, 2H), 5.18 (s, 2H), 4.59–4.53 (m, 3H), 4.44 (t, J = 8.2 Hz, 1H), 4.36–4.32 (m, 2H), 4.25 (dd, J = 15.7, 5.7 Hz, 1H), 3.94 (d, J = 2.8 Hz, 2H), 3.84 (t, J = 5.4 Hz, 2H), 3.65 (dd, J = 10.7, 3.9 Hz, 1H), 3.61 (s, 1H), 3.60–3.52 (m, 5H), 2.42 (s, 3H), 2.06 (ddd, J = 9.1, 7.6, 3.9 Hz, 1H), 1.89 (ddd, J = 13.1, 9.0, 4.5 Hz, 1H), 0.91 (s, 9H). ESI-MS m/z: 1061.2 (MH^+), 531.3 $(MH_2)^{2+}$. HRMS calcd. for $C_{57}H_{61}N_{10}O_9S$ (MH^+), 1061.4338; found, 1061.4331. HRMS calcd. for $C_{57}H_{62}N_{10}O_9S$ $(MH_2)^{2+}$, 531.2205; found, 531.2196.

4-((2-(4-((1-((*S*)-13-((2*S*,4*R*)-4-Hydroxy-2-((4-(4-methylthiazol-5-yl)benzyl)carbamoyl)pyrrolidine-1-carbonyl)-14,14-dimethyl-11-oxo-3,6,9-trioxa-12-azapentadecyl)-1*H*-1,2,3-triazol-4-yl)methoxy)phenyl)-7-phenylimidazo[1,2-*a*]pyridin-3-yl)amino)benzoic acid (5b). Treatment of 4-((7-phenyl-2-(4-(prop-2-yn-1-yloxy)phenyl)imidazo[1,2-*a*]pyridin-3-yl)amino)benzoic acid (**6b**)[24] and commercially available (2*S*,4*R*)-1-((*S*)-14-azido-2-(*tert*-butyl)-4-oxo-6,9,12-trioxa-3-azatetradecanoyl)-4-hydroxy-*N*-(4-(4-methylthiazol-5-yl)benzyl)pyrrolidine-2-carboxamide (**8b**) as outlined in general procedure A and purification by preparative HPLC (CAT# 00F-4436-U0-AX) (linear gradient of 20% B to 50% B over 20 min with a flow rate 20 mL min^{-1}, retention time = 15.3 min) provided the title compound (**5b**) as a white fluffy solid (42% yield).

^{1}H NMR (500 MHz, DMSO-d_6) ^{1}H NMR (500 MHz, DMSO) δ 12.45 (brs, 1H), 9.08 (s, 1H), 8.97 (s, 1H), 8.60 (t, J = 6.1 Hz, 1H), 8.33 (d, J = 7.1 Hz, 1H), 8.19 (s, 1H), 8.09 (s, 1H), 7.93–7.86 (m, 4H), 7.80–7.76 (m, 2H), 7.69 (d, J = 7.2 Hz, 1H), 7.59 (dd, J = 8.3, 6.6 Hz, 2H), 7.53 (dd, J = 8.4, 6.1 Hz, 1H), 7.43 (d, J = 9.3 Hz, 1H), 7.38 (s, 4H), 7.20 (d, J = 9.0 Hz, 2H), 6.76 (d, J = 8.2 Hz, 2H), 5.18 (s, 2H), 4.56 (d, J = 9.6 Hz, 1H), 4.51 (t, J = 5.2 Hz, 2H), 4.43 (t, J = 8.2 Hz, 1H), 4.36 (dd, J = 15.7, 6.2 Hz, 2H), 4.24 (dd, J = 15.8, 5.7 Hz, 1H), 3.94 (s, 2H), 3.79 (t, J = 5.2 Hz, 2H), 3.66 (dd, J = 10.7, 3.9 Hz, 2H), 3.61–3.50 (m, 9H), 2.43 (s, 3H), 2.06 (ddd, J = 9.5, 7.1, 4.3 Hz, 1H), 1.89 (ddt, J = 13.1, 8.9, 4.4 Hz, 1H), 0.92 (s, 9H). ESI-MS m/z: 1105.2 (MH^+). HRMS calcd. for $C_{59}H_{65}N_{10}O_{10}S$ (MH^+), 1105.4600; found, 1105.2327. HRMS calcd. for $C_{59}H_{66}N_{10}O_{10}S$ $(MH_2)^{2+}$, 553.2337; found, 553.2327.

4-((2-(4-((1-((*S*)-16-((2*S*,4*R*)-4-Hydroxy-2-((4-(4-methylthiazol-5-yl)benzyl)carbamoyl)pyrrolidine-1-carbonyl)-17,17-dimethyl-14-oxo-3,6,9,12-tetraoxa-15-azaoctadecyl)-1*H*-1,2,3-triazol-4-yl)methoxy)phenyl)-7-phenylimidazo[1,2-*a*]pyridin-3-yl)amino)benzoic acid (5c). Treatment of 4-((7-phenyl-2-(4-(prop-2-yn-1-yloxy)phenyl)imidazo[1,2-*a*]pyridin-3-yl)amino)benzoic acid (**6b**)[24] and commercially available (2*S*,4*R*)-1-((*S*)-17-azido-2-(*tert*-butyl)-4-oxo-6,9,12,15-tetraoxa-3-azaheptadecanoyl)-4-hydroxy-*N*-(4-(4-methylthiazol-5-yl)benzyl)pyrrolidine-2-carboxamide (**8c**) as outlined in general procedure A and purification by preparative HPLC (CAT# 00F-4436-U0-AX) (linear gradient of 30% B to 35% B over 20 min with a flow rate 20 mL min^{-1}, retention time = 13.9 min) provided the title compound (**5c**) as a white fluffy solid (53% yield). ^{1}H NMR (500 MHz, DMSO-d_6) δ 12.42 (brs, 1H), 9.05 (s, 1H), 8.97 (s, 1H), 8.61 (t, J = 6.1 Hz, 1H), 8.29 (d, J = 5.8 Hz, 1H), 8.20 (s, 1H), 8.08 (s, 1H), 7.90 (dd, J = 8.0, 3.4 Hz, 4H), 7.78 (d, J = 9.1 Hz, 2H), 7.64 (d, J = 6.4 Hz, 1H), 7.58 (t, J = 7.4 Hz, 2H), 7.55–7.50 (m, 1H), 7.45–7.40 (m, 2H), 7.39 (s, 4H), 7.19 (d, J = 8.9 Hz, 2H), 6.75 (d, J = 8.1 Hz, 2H), 5.18 (s, 2H), 4.56 (d, J = 9.6 Hz, 1H), 4.52 (t, J = 5.2 Hz, 2H), 4.43 (t, J = 8.2 Hz, 1H), 4.41–4.33 (m, 2H), 4.24 (dd, J = 15.8, 5.7 Hz, 1H), 3.95 (s, 2H), 3.79 (t, J = 5.2 Hz, 2H), 3.66 (dd, J = 10.7, 3.9 Hz, 1H), 3.62–3.55 (m, 3H), 3.54–3.51 (m, 3H), 3.51–3.45 (m, 5H), 3.45–3.42 (m, 2H), 2.43 (s, 3H), 2.06 (ddd, J = 9.5, 7.6, 3.8 Hz, 1H), 1.89 (ddd, J = 13.0, 8.8, 4.5 Hz, 1H), 0.93 (s, 9H). ESI-MS m/z: 1149.3 (MH^+). HRMS calcd. for $C_{61}H_{69}N_{10}O_{11}S$ (MH^+), 1149.4863; found, 1149.4847. HRMS calcd. for $C_{61}H_{70}N_{10}O_{11}S$ $(MH_2)^{2+}$, 575.2468; found, 575.2457.

4-((2-(4-((1-(4-(2-((2-(2,6-Dioxopiperidin-3-yl)-1,3-dioxoisoindolin-4-yl)oxy)acetamido)butyl)-1*H*-1,2,3-triazol-4-yl)methoxy)phenyl)-7-phenylimidazo[1,2-*a*]pyridin-3-yl)amino)benzoic acid (5d). Treatment of 4-((7-phenyl-2-(4-(prop-2-yn-1-yloxy)phenyl)imidazo[1,2-*a*]pyridin-3-yl)amino)benzoic acid (**6b**)[24] and commercially available *N*-(4-azidobutyl)-2-((2-(2,6-dioxopiperidin-3-yl)-1,3-dioxoisoindolin-4-yl)oxy)acetamide (**9a**) as outlined in general procedure A and purification by preparative HPLC (CAT# 00F-4436-U0-AX) (linear gradient of 30% B to 35% B over 20 min with a flow rate 20 mL min^{-1}, retention time = 12.6 min) provided the title compound (**5d**) as a white fluffy solid (55% yield). ^{1}H NMR (500 MHz, DMSO-d_6) δ 11.13 (s, 1H), 9.06 (s, 1H), 8.23 (s, 1H), 8.07 (s, 1H), 8.03 (t, J = 5.8 Hz, 1H), 7.90 (td, J = 6.0, 3.3 Hz, 4H), 7.81–7.76 (m, 3H), 7.68–7.62 (m, 1H), 7.58 (t, J = 7.5 Hz, 2H), 7.55–7.50 (m, 1H), 7.48 (d, J = 7.3 Hz, 1H), 7.37 (d, J = 8.5 Hz, 1H), 7.22–7.17 (m, 2H), 6.75 (d, J = 8.2 Hz, 2H), 5.18 (s, 2H), 5.11 (dd, J = 12.8, 5.4 Hz, 1H), 4.77 (s, 2H), 4.37 (t, J = 7.1 Hz, 2H), 3.17 (q, J = 6.6 Hz, 2H), 2.89 (ddd, J = 16.9, 13.8, 5.5 Hz, 1H), 2.59 (dq, J = 19.5, 3.3 Hz, 1H), 2.54 (s, 1H), 2.03 (ddd, J = 10.5,

5.5, 3.1 Hz, 1H), 1.81 (dq, J = 9.8, 7.2 Hz, 2H), 1.40 (dq, J = 9.9, 7.1 Hz, 2H). ESI-MS m/z: 888.1 (MH^+). HRMS calcd. for $C_{48}H_{42}N_9O_9$ (MH^+), 888.3100; found, 888.3076. HRMS calcd. for $C_{48}H_{43}N_9O_9$ $(MH_2)^{2+}$, 444.6586; found, 444.6572.

4-((2-(4-((1-(4-(2-((2-(2,6-Dioxopiperidin-3-yl)-1,3-dioxoisoindolin-4-yl)oxy)acetamido)butyl)-1*H*-1,2,3-triazol-4-yl)methoxy)phenyl)imidazo[1,2-*a*]pyridin-3-yl)amino)benzoic acid (5e). Treatment of 4-((2-(4-(prop-2-yn-1-yloxy)phenyl)imidazo[1,2-*a*]pyridin-3-yl)amino)benzoic acid (**6c**)[24] and commercially available *N*-(4-azidobutyl)-2-((2-(2,6-dioxopiperidin-3-yl)-1,3-dioxoisoindolin-4-yl)oxy)acetamide (**9a**) as outlined in general procedure A and purification by preparative HPLC (CAT# 00F-4436-U0-AX) (linear gradient of 30% B to 35% B over 20 min with a flow rate 20 mL min^{-1}, retention time = 13.2 min) provided the title compound (**5e**) as a white fluffy solid (55% yield).^{1}H NMR (500 MHz, DMSO-d_6) δ 11.13 (s, 1H), 9.05 (s, 1H), 8.29 (d, J = 6.6 Hz, 1H), 8.23 (s, 1H), 8.03 (t, J = 5.8 Hz, 1H), 7.91 (d, J = 9.0 Hz, 1H), 7.86 (d, J = 8.9 Hz, 2H), 7.81–7.75 (m, 3H), 7.48 (d, J = 7.2 Hz, 1H), 7.37 (d, J = 8.6 Hz, 1H), 7.33 (s, 1H), 7.20 (d, J = 8.9 Hz, 2H), 6.73 (d, J = 8.1 Hz, 2H), 5.17 (s, 2H), 5.11 (dd, J = 12.8, 5.4 Hz, 1H), 4.77 (s, 2H), 4.37 (t, J = 7.1 Hz, 2H), 3.17 (q, J = 6.6 Hz, 2H), 2.89 (ddd, J = 16.9, 13.9, 5.5 Hz, 1H), 2.64–2.54 (m, 2H), 2.03 (dtd, J = 10.5, 5.3, 2.6 Hz, 1H), 1.81 (dq, J = 9.6, 7.1 Hz, 2H), 1.40 (dq, J = 9.8, 7.0 Hz, 2H). ESI-MS m/z: 812.2 (MH^+). HRMS calcd. for $C_{42}H_{38}N_9O_9$ (MH^+), 812.2787; found, 812.2762. HRMS calcd. for $C_{42}H_{39}N_9O_9$ $(MH_2)^{2+}$, 406.6430; found, 406.6415.

4-((2-(4-(1-(4-(2-((2-(2,6-Dioxopiperidin-3-yl)-1,3-dioxoisoindolin-4-yl)oxy)acetamido)butyl)-1*H*-1,2,3-triazol-4-yl)phenyl)-7-phenylimidazo[1,2-*a*]pyridin-3-yl)amino)benzoic acid (5f). Treatment of 4-((2-(4-ethynylphenyl)-7-phenylimidazo[1,2-*a*]pyridin-3-yl)amino)benzoic acid (**6d**)[24] and commercially available *N*-(4-azidobutyl)-2-((2-(2,6-dioxopiperidin-3-yl)-1,3-dioxoisoindolin-4-yl)oxy)acetamide (**9a**) as outlined in general procedure A and purification by preparative HPLC (CAT# 00F-4436-U0-AX) (linear gradient of 30% B to 35% B over 20 min with a flow rate 20 mL min^{-1}, retention time = 13.3 min) provided the title compound (**5f**) as a white fluffy solid (33% yield). ^{1}H NMR (500 MHz, DMSO-d_6) δ 11.12 (s, 1H), 9.07 (s, 1H), 8.61 (s, 1H), 8.25 (d, J = 7.1 Hz, 1H), 8.10–8.01 (m, 4H), 7.94 (d, J = 8.1 Hz, 2H), 7.90 (d, J = 7.2 Hz, 2H), 7.82–7.75 (m, 3H), 7.57 (t, J = 7.5 Hz, 3H), 7.50 (dd, J = 8.4, 6.2 Hz, 1H), 7.47 (d, J = 7.2 Hz, 1H), 7.37 (d, J = 8.5 Hz, 1H), 6.73 (d, J = 7.5 Hz, 2H), 5.11 (dd, J = 12.8, 5.4 Hz, 1H), 4.77 (s, 2H), 4.42 (t, J = 7.0 Hz, 2H), 3.19 (q, J = 6.6 Hz, 2H), 2.88 (ddd, J = 16.9, 13.9, 5.5 Hz, 1H), 2.65–2.52 (m, 3H), 2.02 (ddq, J = 10.6, 5.5, 2.5 Hz, 1H), 1.86 (p, J = 7.2 Hz, 2H), 1.44 (p, J = 7.0 Hz, 2H). ESI-MS m/z: 858.3 (MH^+). HRMS calcd. for $C_{47}H_{40}N_9O_8$ (MH^+), 858.2994; found, 858.2990. HRMS calcd. for $C_{47}H_{41}N_9O_8$ $(MH_2)^{2+}$, 429.6534; found, 429.6529.

4-((2-(4-(1-(4-(2-((2-(2,6-Dioxopiperidin-3-yl)-1,3-dioxoisoindolin-4-yl)oxy)acetamido)butyl)-1*H*-1,2,3-triazol-4-yl)phenyl)imidazo[1,2-*a*]pyridin-3-yl)amino)benzoic acid (5g). Treatment of 4-((2-(4-ethynylphenyl)imidazo[1,2-*a*]pyridin-3-yl)amino)benzoic acid (**6e**)[24] and commercially available *N*-(4-azidobutyl)-2-((2-(2,6-dioxopiperidin-3-yl)-1,3-dioxoisoindolin-4-yl)oxy)acetamide (**9a**) as outlined in general procedure A and purification by preparative HPLC (CAT# 00F-4436-U0-AX) (linear gradient of 20% B to 25% B over 20 min with a flow rate 20 mL min^{-1}, retention time = 12.5 min) provided the title compound (**5g**) as a white fluffy solid (47% yield). ^{1}H NMR (500 MHz, DMSO-d_6) δ 11.12 (s, 1H), 9.08 (s, 1H), 8.61 (s, 1H), 8.26 (d, J = 6.8 Hz, 1H), 8.06–7.99 (m, 3H), 7.95 (d, J = 8.5 Hz, 2H), 7.88 (d, J = 9.0 Hz, 1H), 7.81–7.70 (m, 4H), 7.46 (d, J = 7.2 Hz, 1H), 7.37 (d, J = 8.5 Hz, 1H), 7.27 (s, 1H), 6.72 (d, J = 8.0 Hz, 2H), 5.11 (dd, J = 12.8, 5.4 Hz, 1H), 4.77 (s, 2H), 4.42 (t, J = 7.0 Hz, 2H), 3.19 (q, J = 6.6 Hz, 2H), 2.88 (ddd, J = 16.9, 13.9, 5.5 Hz, 1H), 2.59 (dt, J = 18.6, 4.1 Hz, 1H), 2.02 (dtd, J = 10.4, 5.2, 2.5 Hz, 1H), 1.86 (dq, J = 9.4, 7.0 Hz, 2H), 1.43 (dq, J = 9.7, 7.0 Hz, 2H). ESI-MS m/z: 782.2 (MH^+). HRMS calcd. for $C_{41}H_{36}N_9O_8$ (MH^+), 782.2681; found, 782.2684. HRMS calcd. for $C_{41}H_{37}N_9O_9$ $(MH_2)^{2+}$, 391.6377; found, 391.6376.

***tert*-Butyl 4-((2-(4-(hydroxymethyl)phenyl)-7-phenylimidazo[1,2-*a*]pyridin-3-yl)amino)benzoate (17).** The mixture of 4-phenylpyridin-2-amine (**14**, 1.0 g, 5.9 mmol), aldehyde 4-(hydroxymethyl)benzaldehyde (**15**, 0.8 g, 5.9 mmol), acetic acid (0.68 mL, 12 mmol) was stirred in MeOH (10 mL) at rt for 15 min. *tert*-Butyl 4-isocyanobenzoate (**16**, 1.3 g, 5.9 mmol)[24] was added. The yellow solution was stirred at rt for 2 days. The formed white suspension was filtered and washed by water and hexane. Solid product was collected. The filtrate was concentrated and purified by silica gel column using Combiflash. All of the product was combined and the title compound (**17**, 2.3 g, 4.7 mmol) was afforded as a yellow solid (80% yield). ^{1}H NMR (400 MHz, DMSO-d_6) δ 8.87 (s, 1H), 8.03–7.96 (m, 4H), 7.85 (d, J = 7.1 Hz, 2H), 7.72 (d, J = 8.8 Hz, 2H), 7.53 (t, J = 7.6 Hz, 2H), 7.44 (t, J = 7.3 Hz, 1H), 7.34 (dd, J = 9.0, 7.6 Hz, 3H), 6.60 (s, 2H), 5.18 (t, J = 5.5 Hz, 1H), 4.50 (s, 2H), 1.49 (s, 9H). ^{13}C NMR (101 MHz, DMSO-d_6) δ 165.38, 150.20, 142.79, 142.64, 138.83, 138.30, 137.36, 132.22, 131.74 (2C), 129.61 (2C), 128.80, 127.08 (4C), 126.67 (2C), 123.56, 121.84, 117.93, 113.91, 112.94 (2C), 112.26, 80.03, 63.15, 28.38 (3C). DUIS-MS m/z: 492.2 (MH^+), 490.1 ($M–H)^-$.

***tert*-Butyl 4-((2-(4-(bromomethyl)phenyl)-7-phenylimidazo[1,2-*a*]pyridin-3-yl)amino)benzoate (18).** Compounded *tert*-butyl 4-((2-(4-(hydroxymethyl)phenyl)-7-phenylimidazo[1,2-*a*]pyridin-3-yl)amino)benzoate (**17**, 151W-124, 141, 418 mg, 0.85 mmol) was dissolved in THF (9.0 mL). Triphenylphosphine (335 mg, 1.3 mmol) was added. The formed yellow solution was cooled to 0 °C by ice bath. Carbon tetrabromide (424 mg, 1.3 mmol) was added. The reaction mixture was stirred (rt, 0.5 h). After purification by silica gel chromatography. The title compound (**18**, 320 mg) was afforded as a yellow solid (68% yield). ^{1}H NMR (500 MHz, $CDCl_3$) δ 7.90 (d, J = 8.3 Hz, 2H), 7.84 (d, J = 8.9 Hz, 2H), 7.73 (d, J = 7.2 Hz, 2H), 7.57 (dd, J = 8.4, 1.4 Hz, 2H), 7.45 (t, J = 7.5 Hz, 2H), 7.41–7.36 (m, 1H), 7.30 (d, J = 8.4 Hz, 2H), 6.99 (dd, J = 6.9, 1.9 Hz, 1H), 6.56 (d, J = 8.3 Hz, 2H), 6.50 (s, 1H), 4.43 (s, 2H), 1.54 (s, 9H). ^{13}C NMR (126 MHz, $CDCl_3$) δ 165.65, 148.46, 143.24, 139.34, 138.50,

138.30, 137.36, 133.13, 131.77 (2C), 129.32 (2C), 129.13 (2C), 128.43, 127.18 (2C), 126.70 (2C), 123.50, 122.53, 117.20, 114.14, 112.62 (2C), 112.40, 80.40, 33.45, 28.24 (3C). ESI-MS *m*/*z*: 554.10, 556.10 (MH^+).

***tert*-Butyl 4-((2-(4-(azidomethyl)phenyl)-7-phenylimidazo[1,2-*a*]pyridin-3-yl)amino)benzoate (7).** Compound *tert*-butyl 4-((2-(4-(bromomethyl)phenyl)-7-phenylimidazo[1,2-*a*]pyridin-3-yl) amino)benzoate (**18**, 360 mg, 0.65 mmol) was dissolved in acetone (5.0 mL) and water (1.0 mL). Sodium azide (127 mg, 1.95 mmol) was added. The mixture was stirred (55 °C, 18 h). The reaction mixture was concentrated and purified by silica gel chromatography. The title compound (**7**, 143 mg) was afforded as a white solid (43% yield). ^{1}H NMR (500 MHz, $CDCl_3$) δ 7.96 (d, J = 8.3 Hz, 2H), 7.86 (d, J = 8.7 Hz, 2H), 7.80–7.76 (m, 2H), 7.61 (dd, J = 8.3, 1.3 Hz, 2H), 7.47 (t, J = 7.6 Hz, 2H), 7.42–7.38 (m, 1H), 7.30–7.26 (m, 2H), 7.04 (dd, J = 7.1, 1.8 Hz, 1H), 6.59 (d, J = 8.4 Hz, 2H), 6.27 (s, 1H), 4.31 (s, 2H), 1.55 (s, 9H). ^{13}C NMR (126 MHz, $CDCl_3$) δ 165.63, 148.42, 143.34, 139.61, 138.55, 138.38, 135.12, 133.06, 131.83 (2C), 129.15 (2C), 128.49 (2C), 128.45, 127.32 (2C), 126.75 (2C), 123.69, 122.48, 116.98, 114.33, 112.66 (2C), 112.48, 80.45, 54.55, 28.25 (3C). ESI-MS *m*/*z*: 517.20 (MH^+), 539.20 (MNa^+).

2-(2,6-Dioxopiperidin-3-yl)-4-(prop-2-yn-1-ylamino) isoindoline-1,3-dione (9b). Treatment of 2-(2,6-dioxopiperidin-3-yl)-4-fluoroisoindoline-1,3-dione (**19**) and prop-2-yn-1-amine as outlined in general procedure C and purification by preparative HPLC (CAT# 00G-4436-P0-AX) (linear gradient of 20% B to 65% B over 20 min with a flow rate 20 mL min^{-1}, retention time = 14.1 min) provided the title compound (**9b**) as a white fluffy solid (92% yield). ^{1}H NMR (500 MHz, $CDCl_3$) δ 8.25 (s, 1H), 7.57 (dd, J = 8.5, 7.2 Hz, 1H), 7.22–7.18 (m, 1H), 7.03 (d, J = 8.4 Hz, 1H), 4.93 (dd, J = 12.3, 5.4 Hz, 1H), 4.10 (d, J = 2.5 Hz, 2H), 2.93–2.87 (m, 1H), 2.85–2.70 (m, 2H), 2.28 (t, J = 2.4 Hz, 1H), 2.16–2.10 (m, 1H), 2.01 (s, 1H). ^{13}C NMR (126 MHz, $CDCl_3$) δ 169.24, 167.33, 166.40, 165.56, 143.63, 134.24, 130.48, 115.29, 110.84, 109.44, 77.23, 70.26, 47.01, 30.39, 29.47, 20.82. ESI-MS *m*/*z*: 312.10 (MH^+).

2-(2,6-Dioxopiperidin-3-yl)-4-(methyl(prop-2-yn-1-yl)amino) isoindoline-1,3-dione (9c). Treatment of 2-(2,6-dioxopiperidin-3-yl)-4-fluoroisoindoline-1,3-dione (**19**) and *N*-methylprop-2-yn-1-amine as outlined in general procedure C and purification by silica gel chromatograph provided the title compound (**9c**) as a yellow solid (61% yield). ^{1}H NMR (500 MHz, DMSO-d_6) δ 11.11 (s, 1H), 11.06 (s, 1H), 7.90 (ddd, J = 8.4, 7.3, 4.4 Hz, 1H), 7.75 (d, J = 7.3 Hz, 1H), 7.70 (d, J = 8.0 Hz, 1H), 7.69–7.65 (m, 2H), 7.34 (s, 1H), 7.32 (s, 1H), 5.12 (dd, J = 12.9, 5.4 Hz, 1H), 5.07 (dd, J = 12.7, 5.5 Hz, 1H), 4.28 (d, J = 2.4 Hz, 2H), 3.30 (s, 2H), 3.18 (t, J = 2.3 Hz, 1H), 2.97 (s, 3H), 2.90–2.80 (m, 3H), 2.60–2.52 (m, 3H), 2.48–2.43 (m, 3H), 2.02 (dddd, J = 12.2, 9.4, 5.9, 2.3 Hz, 2H). DUIS-MS *m*/*z*: 326.1 (MH^+).

4-(But-3-yn-1-ylamino)-2-(2,6-dioxopiperidin-3-yl)isoindoline-1,3-dione (9d). Treatment of 2-(2,6-dioxopiperidin-3-yl)-4-fluoroisoindoline-1,3-dione (**19**) and but-3-yn-1-amine as outlined in general procedure C and purification by silica gel chromatograph provided the title compound (**9d**) as a yellow solid (52% yield). ^{1}H NMR (500 MHz, $CDCl_3$) δ 7.98 (s, 1H), 7.52 (dd, J = 8.5, 7.1 Hz, 1H), 7.14 (d, J = 7.1 Hz, 1H), 6.93 (d, J = 8.5 Hz, 1H), 6.49 (s, 1H), 4.92 (dd, J = 12.4, 5.4 Hz, 1H), 3.49 (q, J = 5.7, 4.5 Hz, 2H), 2.92–2.69 (m, 4H), 2.55 (td, J = 6.9, 2.6 Hz, 2H), 2.16–2.10 (m, 1H), 2.08 (t, J = 2.6 Hz, 1H). ^{13}C NMR (126 MHz, $CDCl_3$) δ 170.82, 169.31, 168.15, 167.50, 146.37, 136.20, 132.58, 116.51, 112.03, 110.57, 80.61, 70.77, 48.90, 41.29, 31.42, 22.77, 19.38. ESI-MS *m*/*z*: 326.10 (MH^+).

***tert*-Butyl 4-((2-(4-((4-(((2-(2,6-dioxopiperidin-3-yl)-1,3-dioxoisoindolin-4-yl)amino)methyl)-1*H*-1,2,3-triazol-1-yl) methyl)phenyl)-7-phenylimidazo[1,2-*a*]pyridin-3-yl)amino) benzoate (20a).** Treatment of (*tert*-butyl 4-((2-(4-(azidomethyl) phenyl)-7-phenylimidazo[1,2-*a*]pyridin-3-yl)amino)benzoate (**7**) and 2-(2,6-dioxopiperidin-3-yl)-4-(prop-2-yn-1-ylamino) isoindoline-1,3-dione (**9b**) as outlined in general procedure A (rt, 18 h) and purification by preparative HPLC (CAT# 00G-4436-P0-AX) (linear gradient of 20% B to 60% B over 20 min with a flow rate 20 mL min^{-1}, retention time = 18.6 min) provided the title compound (**20a**) as a yellow fluffy solid (60% yield). ^{1}H NMR (500 MHz, DMSO-d_6) δ 11.10 (s, 1H), 9.05 (s, 1H), 8.24 (d, J = 7.1 Hz, 1H), 8.09 (d, J = 2.6 Hz, 2H), 7.90 (t, J = 8.2 Hz, 4H), 7.73 (d, J = 9.0 Hz, 2H), 7.61 (d, J = 7.1 Hz, 1H), 7.58 (t, J = 7.5 Hz, 2H), 7.55–7.49 (m, 2H), 7.39 (d, J = 8.3 Hz, 2H), 7.13 (d, J = 8.6 Hz, 1H), 7.10 (d, J = 6.3 Hz, 1H), 7.04 (d, J = 7.0 Hz, 1H), 6.75–6.66 (m, 2H), 5.60 (s, 2H), 5.05 (dd, J = 12.8, 5.4 Hz, 1H), 4.59 (d, J = 4.7 Hz, 2H), 2.93–2.84 (m, 1H), 2.62–2.51 (m, 2H), 2.02 (ddd, J = 9.8, 5.5, 2.7 Hz, 1H), 1.49 (s, 9H). ESI-MS *m*/*z*: 828.20 (MH^+).

4-((2-(4-((4-(((2-(2,6-Dioxopiperidin-3-yl)-1,3-dioxoisoindolin-4-yl)amino)methyl)-1*H*-1,2,3-triazol-1-yl) methyl)phenyl)-7-phenylimidazo[1,2-*a*]pyridin-3-yl)amino) benzoic acid (5h). Treatment of *tert*-butyl 4-((2-(4-((4-(((2-(2,6-dioxopiperidin-3-yl)-1,3-dioxoisoindolin-4-yl)amino)methyl)-1*H*-1,2,3-triazol-1-yl)methyl)phenyl)-7-phenylimidazo[1,2-*a*] pyridin-3-yl)amino)benzoate (**20a**) as outlined in general procedure B and purification by preparative HPLC (CAT# 00G-4436-P0-AX) (linear gradient of 20% B to 60% B over 20 min with a flow rate 20 mL min^{-1}, retention time = 13.4 min) provided the title compound (**5h**) as a yellow fluffy solid (77% yield). ^{1}H NMR (500 MHz, DMSO-d_6) δ 11.12 (s, 1H), 9.08 (s, 1H), 8.31 (d, J = 7.1 Hz, 1H), 8.12 (s, 2H), 7.94 (dd, J = 14.6, 7.7 Hz, 4H), 7.80 (d, J = 8.5 Hz, 2H), 7.65 (d, J = 7.2 Hz, 1H), 7.61 (t, J = 7.5 Hz, 2H), 7.55 (q, J = 8.0 Hz, 2H), 7.42 (d, J = 8.1 Hz, 2H), 7.17 (d, J = 8.6 Hz, 1H), 7.11 (d, J = 6.4 Hz, 1H), 7.07 (d, J = 7.1 Hz, 1H), 6.75 (d, J = 8.2 Hz, 2H), 5.63 (s, 2H), 5.08 (dd, J = 12.8, 5.4 Hz, 1H), 4.62 (d, J = 4.5 Hz, 2H), 2.91 (ddd, J = 16.9, 13.8, 5.4 Hz, 1H), 2.65–2.55 (m, 2H), 2.05 (dp, J = 10.6, 3.2 Hz, 1H). ESI-MS *m*/*z*: 772.3 (MH^+). HRMS calcd. for $C_{43}H_{34}N_9O_6$ (MH^+), 772.2627; found, 772.2625.

***tert*-Butyl 4-((2-(4-((4-(((2-(2,6-dioxopiperidin-3-yl)-1,3-dioxoisoindolin-4-yl)(methyl)amino)methyl)-1*H*-1,2,3-triazol-1-yl)methyl)phenyl)-7-phenylimidazo[1,2-*a*]pyridin-3-yl)amino) benzoate (20b).** Treatment of (*tert*-butyl 4-((2-(4-(azidomethyl) phenyl)-7-phenylimidazo[1,2-*a*]pyridin-3-yl)amino)benzoate (**7**) and 2-(2,6-dioxopiperidin-3-yl)-4-(methyl(prop-2-yn-1-yl)

amino)isoindoline-1,3-dione (**9c**) as outlined in general procedure A (rt, 18 h) and purification by preparative HPLC (CAT# 00G-4436-P0-AX) (linear gradient of 20% B to 70% B over 20 min with a flow rate 20 mL min^{-1}, retention time = 16.2 min) provided the title compound (**20b**) as a yellow solid (47% yield). ^{1}H NMR (500 MHz, DMSO-d_6) δ 11.09 (s, 1H), 9.04 (s, 1H), 8.23 (d, J = 7.2 Hz, 1H), 8.07 (t, J = 1.2 Hz, 1H), 8.06 (s, 1H), 7.90 (t, J = 7.6 Hz, 4H), 7.73 (d, J = 9.1 Hz, 2H), 7.60–7.56 (m, 4H), 7.53–7.49 (m, 1H), 7.30 (d, J = 8.3 Hz, 2H), 7.27 (dd, J = 12.7, 7.8 Hz, 2H), 6.71 (s, 2H), 5.60 (s, 2H), 5.10 (dd, J = 12.9, 5.4 Hz, 1H), 4.75 (s, 2H), 2.95 (s, 3H), 2.88 (ddd, J = 17.4, 14.1, 5.5 Hz, 1H), 2.61–2.56 (m, 1H), 2.56–2.52 (m, 1H), 2.05–1.99 (m, 1H), 1.49 (s, 9H). ESI-MS m/z: 842.20 (MH^+).

4-((2-(4-((4-(((2-(2,6-Dioxopiperidin-3-yl)-1,3-dioxoisoindolin-4-yl)(methyl)amino)methyl)-1*H*-1,2,3-triazol-1-yl)methyl)phenyl)-7-phenylimidazo[1,2-*a*]pyridin-3-yl)amino) benzoic acid (5i). Treatment of *tert*-butyl 4-((2-(4-((4-(((2-(2,6-dioxopiperidin-3-yl)-1,3-dioxoisoindolin-4-yl)(methyl)amino) methyl)-1*H*-1,2,3-triazol-1-yl)methyl)phenyl)-7-phenylimidazo[1,2-*a*]pyridin-3-yl)amino)benzoate (**20b**) as outlined in general procedure B and purification by preparative HPLC (CAT# 00G-4436-P0-AX) (linear gradient of 20% B to 60% B over 20 min with a flow rate 20 mL min^{-1}, retention time = 12.9 min) provided the title compound (**5i**) as a yellow fluffy solid (79% yield). ^{1}H NMR (500 MHz, DMSO-d_6) δ 11.09 (s, 1H), 9.04 (s, 1H), 8.27 (d, J = 7.1 Hz, 1H), 8.07 (d, J = 12.8 Hz, 2H), 7.91 (dd, J = 11.4, 7.9 Hz, 4H), 7.78 (d, J = 8.4 Hz, 2H), 7.61 (d, J = 6.8 Hz, 1H), 7.58 (t, J = 7.7 Hz, 3H), 7.51 (t, J = 7.3 Hz, 1H), 7.33–7.28 (m, 3H), 7.28–7.23 (m, 2H), 6.72 (d, J = 8.2 Hz, 2H), 5.60 (s, 2H), 5.10 (dd, J = 12.9, 5.4 Hz, 1H), 4.75 (s, 2H), 2.88 (ddd, J = 18.3, 14.0, 5.5 Hz, 1H), 2.65–2.52 (m, 2H), 2.06–1.98 (m, 1H). ESI-MS m/z: 786.4 (MH^+). HRMS calcd. for $C_{44}H_{36}N_9O_6$ (MH^+), 786.2783; found, 786.2786.

***tert*-Butyl 4-((2-(4-((4-(2-((2-(2,6-dioxopiperidin-3-yl)-1,3-dioxoisoindolin-4-yl)amino)ethyl)-1*H*-1,2,3-triazol-1-yl)methyl) phenyl)-7-phenylimidazo[1,2-*a*]pyridin-3-yl)amino)benzoate (20c).** Treatment of (*tert*-butyl 4-((2-(4-(azidomethyl)phenyl)-7-phenylimidazo[1,2-*a*]pyridin-3-yl)amino)benzoate (7) and (4-(but-3-yn-1-ylamino)-2-(2,6-dioxopiperidin-3-yl)isoindoline-1,3-dione (**9d**) as outlined in general procedure A (rt, 18 h) and purification by preparative HPLC (CAT# 00G-4436-P0-AX) (linear gradient of 30% B to 60% B over 20 min with a flow rate 20 mL min^{-1}, retention time = 16.4 min) provided the title compound (**20c**) as a yellow solid (50% yield). ^{1}H NMR (500 MHz, DMSO-d_6) δ 11.11 (s, 1H), 9.08 (s, 1H), 8.28 (d, J = 7.1 Hz, 1H), 8.13–8.09 (m, 1H), 8.03 (s, 1H), 7.91 (dd, J = 7.7, 4.8 Hz, 4H), 7.73 (d, J = 9.1 Hz, 2H), 7.66 (d, J = 7.2 Hz, 1H), 7.59 (t, J = 7.5 Hz, 2H), 7.54 (dd, J = 8.3, 7.3 Hz, 2H), 7.40 (d, J = 8.4 Hz, 2H), 7.10 (d, J = 8.6 Hz, 1H), 7.02 (d, J = 7.0 Hz, 1H), 6.73 (d, J = 9.2 Hz, 2H), 5.60 (s, 2H), 5.05 (dd, J = 12.8, 5.4 Hz, 1H), 3.59 (d, J = 5.9 Hz, 2H), 2.94 (t, J = 7.0 Hz, 2H), 2.91–2.82 (m, 1H), 2.62–2.55 (m, 1H), 2.55–2.51 (m, 2H), 2.01 (dtd, J = 12.9, 5.2, 2.2 Hz, 1H), 1.49 (s, 9H). ESI-MS m/z: 842.20 (MH^+).

4-((2-(4-((4-(2-((2-(2,6-Dioxopiperidin-3-yl)-1,3-dioxoisoindolin-4-yl)amino)ethyl)-1*H*-1,2,3-triazol-1-yl)methyl)phenyl)-7-phenylimidazo[1,2-*a*]pyridin-3-yl)amino)benzoic acid (5j). Treatment of *tert*-butyl 4-((2-(4-((4-(2-((2-(2,6-dioxopiperidin-3-yl)-1,3-dioxoisoindolin-4-yl)amino)ethyl)-1*H*-1,2,3-triazol-1-yl) methyl)phenyl)-7-phenylimidazo[1,2-*a*]pyridin-3-yl)amino) benzoate (**20c**) as outlined in general procedure B and purification by preparative HPLC (CAT# 00G-4436-P0-AX) (linear gradient of 20% B to 60% B over 20 min with a flow rate 20 mL min^{-1}, retention time = 13.4 min) provided the title compound (**5j**) as a yellow fluffy solid (91% yield). ^{1}H NMR (500 MHz, DMSO-d_6) δ 11.12 (s, 1H), 9.06 (s, 1H), 8.28 (d, J = 7.1 Hz, 1H), 8.10 (s, 1H), 8.03 (s, 1H), 7.94 (d, J = 8.1 Hz, 2H), 7.90 (d, J = 7.6 Hz, 2H), 7.77 (d, J = 8.6 Hz, 2H), 7.62 (d, J = 7.2 Hz, 1H), 7.60–7.55 (m, 2H), 7.55–7.49 (m, 2H), 7.39 (d, J = 8.2 Hz, 2H), 7.10 (d, J = 8.6 Hz, 1H), 7.02 (d, J = 7.0 Hz, 1H), 6.72 (d, J = 8.1 Hz, 3H), 5.59 (s, 2H), 5.05 (dd, J = 12.8, 5.4 Hz, 1H), 3.59 (q, J = 6.3 Hz, 2H), 2.94 (t, J = 7.0 Hz, 2H), 2.91–2.80 (m, 1H), 2.62–2.52 (m, 1H), 2.05–1.98 (m, 1H). ESI-MS m/z: 786.5 (MH^+). HRMS calcd. for $C_{44}H_{36}N_9O_6$ (MH^+), 786.2783; found, 786.2782.

Data availability

The data supporting this article have been included as part of the ESI.†

Author contributions

XZ and TB conceived the study. XZ designed and synthesized the compounds. WW, MM, KA, and YP performed the biological studies. XZ, WW, MM, KA, YP and TB interpreted the data. XZ and TB took the lead in writing the manuscript. All authors have provided critical feedback and approved the final manuscript.

Conflicts of interest

The authors declare that there is no conflict of interest.

Acknowledgements

This work was supported in part by a Staff Scientist/Staff Clinician Research Award (SSSC-RA) and the Intramural Research Program of the NIH, Center for Cancer Research, National Cancer Institute, National Institutes of Health (Z01-BC 006150 and Z01-BC 006198).

References

1 S. Li, C. Vemuri and C. Chen, *Curr. Opin. Struct. Biol.*, 2024, **87**, 102868.
2 B. C. Soren, J. B. Dasari, A. Ottaviani, F. Iacovelli and P. Fiorani, *Cancer Drug Resist.*, 2020, **3**, 18–25.
3 Y. Pommier, Y. Sun, S.-y. N. Huang and J. L. Nitiss, *Nat. Rev. Mol. Cell Biol.*, 2016, **17**, 703–721.
4 A. Tubbs and A. Nussenzweig, *Cell*, 2017, **168**, 644–656.

5 H. U. Barthelmes, M. Habermeyer, M. O. Christensen, C. Mielke, H. Interthal, J. J. Pouliot, F. Boege and D. Marko, *J. Biol. Chem.*, 2004, **279**, 55618–55625.
6 S. N. Huang and Y. Pommier, *Int. J. Mol. Sci.*, 2019, **20**, 3015.
7 S. S. Laev, N. F. Salakhutdinov and O. I. Lavrik, *Bioorg. Med. Chem.*, 2016, **24**, 5017–5027.
8 L. Debéthune, G. Kohlhagen, A. Grandas and Y. Pommier, *Nucleic Acids Res.*, 2002, **30**, 1198–1204.
9 Y. Sun, L. K. Saha, S. Saha, U. Jo and Y. Pommier, *DNA Repair*, 2020, **94**, 102926.
10 Y. Sun, S. Saha, W. Wang, L. K. Saha, S. N. Huang and Y. Pommier, *DNA Repair*, 2020, **89**, 102837.
11 J. J. Pouliot, K. C. Yao, C. A. Robertson and H. A. Nash, *Science*, 1999, **286**, 552–555.
12 H. Interthal, J. J. Pouliot and J. J. Champoux, *Proc. Natl. Acad. Sci. U. S. A.*, 2001, **98**, 12009–12014.
13 G. L. Beretta, G. Cossa, L. Gatti, F. Zunino and P. Perego, *Curr. Med. Chem.*, 2010, **17**, 1500–1508.
14 E. Q. Comeaux and R. C. A. M. van Waardenburg, *Drug Metab. Rev.*, 2014, **46**, 494–507.
15 R. Gao, B. B. Das, R. Chatterjee, O. D. Abaan, K. Agama, R. Matuo, C. Vinson, P. S. Meltzer and Y. Pommier, *DNA Repair*, 2014, **13**, 1–9.
16 J. Murai, S.-y. N. Huang, B. B. Das, T. S. Dexheimer, S. Takeda and Y. Pommier, *J. Biol. Chem.*, 2012, **287**, 12848–12857.
17 Y. Pommier, S.-y. N. Huang, R. Gao, B. B. Das, J. Murai and C. Marchand, *DNA Repair*, 2014, **19**, 114–129.
18 Z. Hu, H.-w. Wang and L.-k. An, *Yaoxue Xuebao*, 2016, **51**, 215–225.
19 F. J. Flett, E. Ruksenaite, L. A. Armstrong, S. Bharati, R. Carloni, E. R. Morris, C. L. Mackay, H. Interthal and J. M. Richardson, *Nat. Commun.*, 2018, **9**, 1–13.
20 G. T. Lountos, X. Z. Zhao, T. R. Burke, E. Kiselev, Y. Pommier, J. E. Tropea, D. Needle and D. S. Waugh, *Nucleic Acids Res.*, 2019, **47**, 10134–10150.
21 Y. Zhang, Y. Li, C. Sun, X. Chen, L. Han, T. Wang, J. Liu, X. Chen and D. Zhao, *Cancers*, 2021, **13**, 4002.
22 X. Z. Zhao, E. Kiselev, G. T. Lountos, W. Wang, J. E. Tropea, D. Needle, T. A. Hilimire, J. S. Schneekloth, D. S. Waugh, Y. Pommier and T. R. Burke, *Chem. Sci.*, 2021, **12**, 3876–3884.
23 X. Z. Zhao, W. Wang, G. T. Lountos, J. E. Tropea, D. Needle, Y. Pommier and T. R. Burke, *Front. Chem.*, 2022, **10**, 910953.
24 X. Z. Zhao, W. Wang, G. T. Lountos, E. Kiselev, J. E. Tropea, D. Needle, Y. Pommier and T. R. Burke, *RSC Chem. Biol.*, 2023, **4**, 334–343.
25 D. R. Davies, H. Interthal, J. J. Champoux and W. G. J. Hol, *Structure*, 2002, **10**, 237–248.
26 D. R. Davies, H. Interthal, J. J. Champoux and W. G. J. Hol, *J. Mol. Biol.*, 2002, **324**, 917–932.
27 S. T. Dexheimer, S. Antony, C. Marchand and Y. Pommier, *Anti-Cancer Agents Med. Chem.*, 2008, **8**, 381–389.
28 R. A. Copeland, *Evaluation of Enzyme Inhibitors in Drug Discovery*, John Wiley & Sons, Inc., Hoboken, New Jersey, 2nd edn, 2013.
29 A. Zakharenko, N. Dyrkheeva and O. Lavrik, *Med. Res. Rev.*, 2019, **39**, 1427–1441.
30 E. V. Koldysheva, A. P. Men'shchikova, E. L. Lushnikova, N. A. Popova, V. I. Kaledin, V. P. Nikolin, A. L. Zakharenko, O. A. Luzina, N. F. Salakhutdinov and O. I. Lavrik, *Bull. Exp. Biol. Med.*, 2019, **166**, 661–666.
31 A. L. Zakharenko, O. A. Luzina, D. N. Sokolov, V. I. Kaledin, V. P. Nikolin, N. A. Popova, J. Patel, O. D. Zakharova, A. A. Chepanova, A. Zafar, J. Reynisson, E. Leung, I. K. H. Leung, K. P. Volcho, N. F. Salakhutdinov and O. I. Lavrik, *Eur. J. Med. Chem.*, 2019, **161**, 581–593.
32 O. Luzina, A. Filimonov, A. Zakharenko, A. Chepanova, O. Zakharova, E. Ilina, N. Dyrkheeva, G. Likhatskaya, N. Salakhutdinov and O. Lavrik, *J. Nat. Prod.*, 2020, **83**, 2320–2329.
33 A. L. Zakharenko, M. S. Drenichev, N. S. Dyrkheeva, G. A. Ivanov, V. E. Oslovsky, E. S. Ilina, I. A. Chernyshova, O. I. Lavrik and S. N. Mikhailov, *Molecules*, 2020, **25**, 3694.
34 T. M. Khomenko, A. L. Zakharenko, A. A. Chepanova, E. S. Ilina, O. D. Zakharova, V. I. Kaledin, V. P. Nikolin, N. A. Popova, D. V. Korchagina, J. Reynisson, R. Chand, D. M. Ayine-Tora, J. Patel, I. K. H. Leung, K. P. Volcho, N. F. Salakhutdinov and O. I. Lavrik, *Int. J. Mol. Sci.*, 2019, **21**, 126.
35 E. D. Gladkova, I. V. Nechepurenko, R. A. Bredikhin, A. A. Chepanova, A. L. Zakharenko, O. A. Luzina, E. S. Ilina, N. S. Dyrkheeva, E. M. Mamontova, R. O. Anarbaev, J. Reynisson, K. P. Volcho, N. F. Salakhutdinov and O. I. Lavrik, *Int. J. Mol. Sci.*, 2020, **21**, 7162.
36 O. V. Salomatina, I. I. Popadyuk, A. L. Zakharenko, O. D. Zakharova, A. A. Chepanova, N. S. Dyrkheeva, N. I. Komarova, J. Reynisson, R. O. Anarbaev, N. F. Salakhutdinov, O. I. Lavrik and K. P. Volcho, *Steroids*, 2021, **165**, 108771.
37 N. S. Dyrkheeva, A. S. Filimonov, O. A. Luzina, A. L. Zakharenko, E. S. Ilina, A. A. Malakhova, S. P. Medvedev, J. Reynisson, K. P. Volcho, S. M. Zakian, N. F. Salakhutdinov and O. I. Lavrik, *Biomolecules*, 2021, **11**, 973.
38 A. L. Zakharenko, O. A. Luzina, A. A. Chepanova, N. S. Dyrkheeva, N. F. Salakhutdinov and O. I. Lavrik, *Int. J. Mol. Sci.*, 2023, **24**, 5781.
39 O. V. Salomatina, T. E. Kornienko, A. L. Zakharenko, N. I. Komarova, C. Achara, J. Reynisson, N. F. Salakhutdinov, O. I. Lavrik and K. P. Volcho, *Molecules*, 2024, **29**, 581.
40 A. Bermingham, E. Price, C. Marchand, A. Chergui, A. Naumova, E. L. Whitson, L. R. H. Krumpe, E. I. Goncharova, J. R. Evans, T. C. McKee, C. J. Henrich, Y. Pommier and B. R. O'Keefe, *SLAS Discovery*, 2017, **22**, 1093–1105.
41 X. Wei, F. T. Wang, M. X. Si-Tu, H. Fan, J. S. Hu, H. Yang, S. Y. Guan, L. K. An and C. X. Zhang, *Mar. Drugs*, 2022, **20**, 443.
42 L. R. H. Krumpe, B. A. P. Wilson, C. Marchand, S. N. Sunassee, A. Bermingham, W. Wang, E. Price, T. Guszczynski, J. A. Kelley, K. R. Gustafson, Y. Pommier, K. J. Rosengren, C. I. Schroeder and B. R. O'Keefe, *J. Am. Chem. Soc.*, 2020, **142**, 21178–21188.
43 X. Z. Zhao, I. A. Barakat, G. T. Lountos, W. Wang, K. Agama, M. R. A. Mahmud, K. F. Suazo, T. Andresson, Y. Pommier and T. R. Burke, *Commun. Chem.*, 2024, **7**, 208.

44 S. L. McGovern, E. Caselli, N. Grigorieff and B. K. Shoichet, *J. Med. Chem.*, 2002, **45**, 1712–1722.
45 K. M. Sakamoto, K. B. Kim, A. Kumagai, F. Mercurio, C. M. Crews and R. J. Deshaies, *Proc. Natl. Acad. Sci. U. S. A.*, 2001, **98**, 8554–8559.
46 Y. Xue, A. A. Bolinger and J. Zhou, *Expert Opin. Drug Discovery*, 2023, **18**, 467–483.
47 A. C. Lai and C. M. Crews, *Nat. Rev. Drug Discovery*, 2017, **16**, 101–114.
48 X. Sun, H. Gao, Y. Yang, M. He, Y. Wu, Y. Song, Y. Tong and Y. Rao, *Signal Transduction Targeted Ther.*, 2019, **4**, 64.
49 R. Li, M. Liu, Z. Yang, J. Li, Y. Gao and R. Tan, *Molecules*, 2022, **27**, 8828.
50 D. Chirnomas, K. R. Hornberger and C. M. Crews, *Nat. Rev. Clin. Oncol.*, 2023, **20**, 265–278.
51 M. Békés, D. R. Langley and C. M. Crews, *Nat. Rev. Drug Discovery*, 2022, **21**, 181–200.
52 R. I. Troup, C. Fallan and M. G. J. Baud, *Explor. Target. Anti-tumor Ther.*, 2020, **1**, 273–312.
53 B. Mostofian, H. J. Martin, A. Razavi, S. Patel, B. Allen, W. Sherman and J. A. Izaguirre, *J. Chem. Inf. Model.*, 2023, **63**, 5408–5432.
54 H. C. Kolb, M. G. Finn and K. B. Sharpless, *Angew. Chem., Int. Ed.*, 2001, **40**, 2004–2021.
55 C. Yang, R. Tripathi and B. Wang, *RSC Chem. Biol.*, 2024, **5**, 189–197.
56 R. Appel, *Angew. Chem., Int. Ed. Engl.*, 1975, **14**, 801–811.
57 D. K. Brownsey, B. C. Rowley, E. Gorobets, B. S. Gelfand and D. J. Derksen, *Chem. Sci.*, 2021, **12**, 4519–4525.
58 E. J. Brettrager, S. M. Cuya, Z. E. Tibbs, J. Zhang, C. N. Falany, S. G. Aller and R. C. A. M. van Waardenburg, *Sci. Rep.*, 2023, **13**, 1377.
59 S. Saha, Y. Sun, S. N. Huang, S. A. Baechler, L. S. Pongor, K. Agama, U. Jo, H. Zhang, Y. C. Tse-Dinh and Y. Pommier, *Cell Rep.*, 2020, **33**, 108569.
60 L. K. Saha, S. Saha, X. Yang, S.-y. N. Huang, Y. Sun, U. Jo and Y. Pommier, *Nat. Commun.*, 2023, **14**, 1925.
61 C. Cecchini, S. Pannilunghi, S. Tardy and L. Scapozza, *Front. Chem.*, 2021, **9**, 672267.
62 E. Rovers and M. Schapira, *Methods Enzymol.*, 2023, **690**, 311–340.
63 E. S. Fischer, K. Böhm, J. R. Lydeard, H. Yang, M. B. Stadler, S. Cavadini, J. Nagel, F. Serluca, V. Acker, G. M. Lingaraju, R. B. Tichkule, M. Schebesta, W. C. Forrester, M. Schirle, U. Hassiepen, J. Ottl, M. Hild, R. E. Beckwith, J. W. Harper, J. L. Jenkins and N. H. Thomä, *Nature*, 2014, **512**, 49–53.
64 A. O. Ruben Abagyan, Eugene Raush, and Maxim Totrov, ICM-Pro User Guide v.3.9, **https://www.molsoft.com/icmpro/**.
65 R. P. Wurz, K. Dellamaggiore, H. Dou, N. Javier, M.-C. Lo, J. D. McCarter, D. Mohl, C. Sastri, J. R. Lipford and V. J. Cee, *J. Med. Chem.*, 2018, **61**, 453–461.
66 C. Steinebach, I. Sosič, S. Lindner, A. Bricelj, F. Kohl, Y. L. D. Ng, M. Monschke, K. G. Wagner, J. Krönke and M. Gütschow, *MedChemComm*, 2019, **10**, 1037–1041.